J.A. van Aken – 4507460

In vitro evaluation of a PEKK and polycarbonate-urea-urethane implant for the treatment of osteochondral defects

TU Delft

In vitro evaluation of a PEKK and poly-carbonate-urea-urethane implant for the treatment of osteochondral defects

J.A. van Aken – 4507460

In partial fulfilment of the requirements for the degree

Master of Science
Biomedical Engineering

Delft University of Technology
To be defended on Thursday October 24, 2019

Supervisor:	Prof. Dr. Ir. Harrie Weinans
Thesis committee:	Prof. Dr. Ir. Harrie Weinans

TU Delft

Preface

Cartilage defects and degenerative joint diseases are the leading cause of disability worldwide. Its impact is only getting worse due to the aging population. Although treatments are available which temporarily reduce symptoms, no functional cure has been found yet. Finding a treatment would therefore be a huge breakthrough in modern medicine and would improve the quality of life of millions of people around the world.

Treatment of osteochondral lesions with osteochondral implants are very promising to fully restore tissue functionality and much research has been done in this field. This thesis project was conducted with the aim of elaborating on the study by Korthagen et al. who studied a polyurethane and PEKK implant in an equine model. This study focuses on a very similar implant and aims to improve the performance of it. All necessary in vitro tests in preparation for future equine in vivo studies were carried out in this project. Additional efforts were devoted to mechanical testing and 3D printing to provide a solid base for more advanced future implants.

This study was performed in collaboration between the UMCU department of Orthopaedics (Prof. Dr. Ir. Harrie Weinans), the Department of Equine Sciences at Utrecht University (Prof. Dr. René van Weeren) and Jointsphere B.V. (Drs. Ward van Buul). I would like to thank all these collaborators without whom this thesis would not have been possible.

Especially, I would like to thank Prof. Dr. Ir. Weinans for being my excellent mentor who always took time out of his very busy schedule to guide me and discuss obstacles with me. His enthusiasm and knowledge truly fuelled my drive to achieve the best results possible. I would also like to particularly thank Dr. Nicoline Korthagen and Ir. Saskia Plomp who both helped and guided me exceptionally with my experiments. I have to acknowledge that the whole blood assay (experiment 7) in this study was completely conducted by Dr. Korthagen without my help and that I am very grateful she allowed me to adopt the results in my thesis.

Lastly, I wish to thank Drs. Ward van Buul and Gied Hermsen from Jointsphere B.V. for their unconditional support and time to discuss anything with respect to this project.

I hope that you enjoy reading this thesis as much as I enjoyed the work that lead to it.

Joris van Aken
Utrecht, October 2019

Contents

Abstract

Cartilage repair remains a major challenge and treatment of osteochondral defects generally results in inferior quality fibrous repair tissue. This study aims to elaborate on the work of Korthagen et al. who developed a thermoplastic polyurethane and polyetherketoneketone implant to treat osteochondral defects. Although promising results were found, Korthagen et al. encountered difficulties binding the neo-tissue to the elastomer part of the implant. The goal of this study is therefore to test potential solutions to improve cell binding properties of the elastomer in vitro, and to optimize the elastomers mechanical properties to mimic native articular cartilage. The newly produced elastomer showed encouraging cell binding properties with multiple cells types. In addition, 3D printing and punching holes in the elastomer part of the implant both have great potential in creating porosity to physically anchor the neo-tissue. The optimal diameter of vertically aligned punched holes was found to be 319 μm. Not only provides this diameter optimal circumstances for cartilage to grow into, it also optimizes anchoring potential. Besides that, 3D printing efforts were found to be promising in creating both excellent cell facilitating properties as well as mechanical properties mimicking that of native articular cartilage. Both punched and 3D printed elastomer samples were tested for toxicity and immune response. Both tests delivered excellent results and no sign of toxicity or adverse immune response was detected. These results combined with the excellent cell binding properties of the elastomer strengthens our confidence in favorable future in vivo outcomes.

1 Introduction and background information

Articular cartilage is a specialized type of hyaline cartilage that covers joint surfaces and provides a low-friction and load-bearing surface for smooth and pain-free joint motion. Together with the underlying subchondral bone, articular cartilage makes up the osteochondral tissue which has a complex hierarchical structure composed of multiple distinct layers, Figure 1 [1]. Its function can be compromised by traumatic injuries and degenerative joint diseases frequently causing pain, impaired function, and limited motion of the joint, creating a significant healthcare burden worldwide [2][3][4]. Unfortunately, spontaneous healing of cartilage after injury is impaired by its avascular nature, limited cellular content, and low metabolic activity [5]. In addition, the complex hierarchical structure and biomechanical properties of the osteochondral tissue makes the challenge for regenerative therapies even larger [6]. Therefore, treatment of osteochondral lesions to fully restore tissue functionality remains a major challenge for orthopaedic surgeons [7].

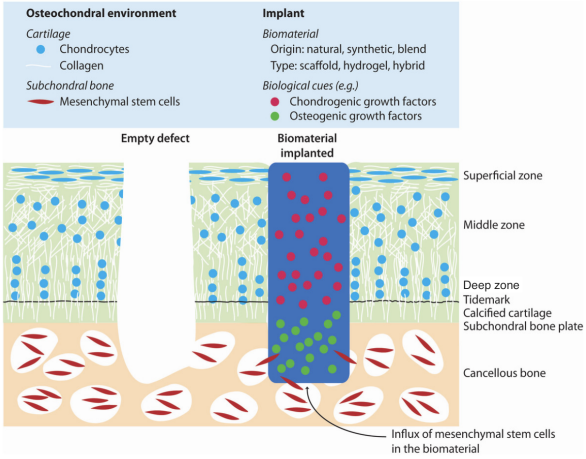

Figure 1: Osteochondral complex hierarchical tissue composition with and without an osteochondral implant [1].

Several techniques are currently used to treat osteochondral defects. For example, bone marrow stimulation by microfracturing or subchondral drilling [6]. Bone marrow is stimulated to release progenitor cells, who have the ability to differentiate into chondrocytes, into the defect [8]. However, instead of producing healthy articular cartilage they generate inferior fibrocartilaginous cartilage resulting in not fully functional tissue which often weakens over time leaving the patient unsatisfied [9]. Other techniques such as autologous chondrocyte transplantation [10], autograft transplantation [11], and allograft transplantation [12] are used too. Although successful in some aspects, each of these techniques has its own limitations. For instance, autograft transplantations suffer from donor site morbidity, degradation of graft tissue and incomplete integration [13]. Allograft transplantations on the other hand present limitations in terms of immune rejection and disease transmission [12]. Overall, the current therapies fail in regenerating osteochondral tissue, leading to hindered motion and promoted progressive degeneration that will lead to the development of osteoarthritis inevitably [7]. Therefore, the need for regeneration therapies of more durable osteochondral tissue persists.

Primarily, regeneration of osteochondral defects was only focused on cartilage repair due to the apparent simplicity and clinical relevance, the underlying subchondral bone was totally neglected at that time [7]. However, osteochondral defects affect multiple tissues due to its complex hierarchical structure consisting of different layer-specific biological and mechanical properties. Filling these osteochondral defects with biological or synthetic implants has lately emerged as one of the most promising treatments, Figure 1 [6][14]. An ideal implant should mimic the biology, architecture, and functional properties of the native osteochondral tissue, in short, be biomimetic. It should also support loading and promote cell attachment, proliferation, and differentiation. Other requirements are biocompatibility and/or bioresorbability [15]. Most studies use bioresobable materials that support the early phases of tissue formation to then be gradually replaced by the regenerative tissue. Permanent implants can scarcely be found in literature [16].

The major advantage of permanent implants is that there is no need for complete osteochondral tissue regeneration as the implant itself delivers all the mechanical and structural properties needed. Besides that, it delivers constant mechanical properties along the way, whereas bioresorbable scaffolds gradually loose their mechanical strength while being replaced by repair tissue. None of the studies found, describes this mechanical trade-off in detail, while this could lead to imbalances and failure of the implant. Accordingly, perhaps in the permanent implant approach lie opportunities for the future of osteochondral defect treatment.

Until recently, osteochondral implants were made out of single phase homogeneous materials, unable to balance chondrogenesis and osteogenesis simultaneously [17]. More recently it was found that multi-layered structures allow for a more accurate mechanical and biological interface [12]. Multilayered biomimetic implants do provide the opportunity to repair multiple tissues simultaneously while providing mechanical properties similar to the native tissue. Among these implants, the biphasic model that combines a bone and cartilage phase is the most common strategy [6]. However, multi-layered and gradient constructs are not uncommon either [18].

The purpose of this study was to continue on the work of Korthagen et al. [19]. Korthagen et al. tested a novel type of osteochondral implant consisting of a base made of polyetherketoneketone (PEKK) that anchors the implant to the native subchondral bone, and an elastomer top layer that consists of a thermoplastic polyurethane, which has mechanical properties approaching articular equine cartilage. The elastomer was loaded with collagen-mimetic peptides 'RGD' (arginine-glycine-aspartic acid) and 'GFOGER' (glycine-phenylalanine-hydroxyproline-glycine-glutamic acid-arginine) which should enhance repair tissue capabilities. The implant was positioned just below the surface of the native articular cartilage which prevented the formation of a large 'step', whilst permitting formation of a layer of neocartilage on the elastomer. The elastomer with its mechanical properties approaching that of native cartilage and the thin (0.5mm) layer of neo-tissue that would be formed on top of it would then result in a filling of the defect with appropriate stiffness [19].

The PEKK and thermoplastic polyurethane implant was both tested in vitro and in vivo by Korthagen et al. Two implants were placed in a created osteochondral defect on the medial femoral trochlear ridge in each stifle of six Shetland ponies where unfilled defects in the contralateral joint served as control. After 12 weeks, the plugs were largely covered with stiff and smooth repair tissue which was well connected to the native cartilage. However, the covering tissue was not connected to the elastomer and was fibrous in nature as it contained negligible amounts of collagen type II and glycosaminoglycans (GAGs). A long-term study with improved cartilage binding properties of the elastomer, including an exercise regimen, was needed to further evaluate the implants potential for clinical use [19].

The goal of this study is therefore to test potential solutions to improve cell binding properties of the elastomer in vitro, and to optimize the elastomers mechanical properties to mimic native articular cartilage. Besides material improvements, to achieve enhanced binding properties, it is necessary to actually anchor the neo-tissue top layer in some way that shear forces would not force the thin tissue layer to detach from the elastomer [20]. Different methods to achieve our goal will be discussed in this report. As the PEKK component of the implant functioned appropriately previously, the current focus will lie completely on optimizing the elastomer part.

2 Materials and methods

For the sake of pleasant reading, all general overlapping materials and methods needed for specific experiments will be described in detail once. Background information on the methods and the reasoning behind them will also be included here, for clarity. Afterwards all unique experiments will be described in the experiments section combining the specific materials and methods directly with the results.

2.1 Elastomer material

The elastomer previously used by Korthagen et al. was more specifically determined as a poly-urethane-urea-hexylene carbonate biomaterial with loaded RGD and GFOGER peptides at the surface. The manufacturer of this material was the company SyMO-Chem B.V. (Eindhoven, the Netherlands). Due to management decisions of Jointsphere B.V.

(Eindhoven, the Netherlands) (owner of the elastomer and commissioning company) this production agreement was terminated and a new contract with Polyvation B.V. (Groningen, the Netherlands) was agreed upon. Polyvation's job was to produce a similar elastomer and optimize the production process. Furthermore, it was decided that no added peptide was needed as it did not yield significant improvements in the previous study. Accordingly, our elastomer material is different from that of Korthagen et al. making all in vitro tests done by Korthagen obsolete for our research. Polyvation's official name for the elastomer was a poly-carbonate-urea-urethane (PCUU).

Simultaneously to our in vitro experiments, the optimisation process of the PCUU was in operation. Due to this, new batches of improved PCUU were delivered to us to test and analyse every other couple of weeks. Five unique batches of PCUU were used in our experiments, differing in production methods and in final intrinsic viscosity (IV), Table 1. As all PCUU alterations could potentially change cell response and mechanical properties, each new batch of PCUU made all previous tests redundant. Eventually, the final PCUU batch (M927) was found to be favorable and reproducible. Accordingly, all decisive in vitro tests were performed or repeated with this PCUU. The PCUU was delivered to the lab in two forms. Firstly, in a press molded disc shape from where smaller discs could be punched for in vitro tests, Figure 2a. Secondly, in tiny grains for 3D printing purposes, Figure 2b.

Table 1: All delivered and used PCUU sample batches, described by distinctive production methods and final intrinsic viscosity (IV) of 125 mg PCUU dissolved in 50 ml 1 volume % trifluoroacetic acid in dichloromethane.

PCUU sample number	**Solvent**	**Catalyst**	**IV(η)**
M524	DMAc	Tin	2.27
M726	DMAc	Tin	1.69
M727	DMSO	Tin	1.67
M901	DMSO	None	1.4
M927	DMSO	None	1.8

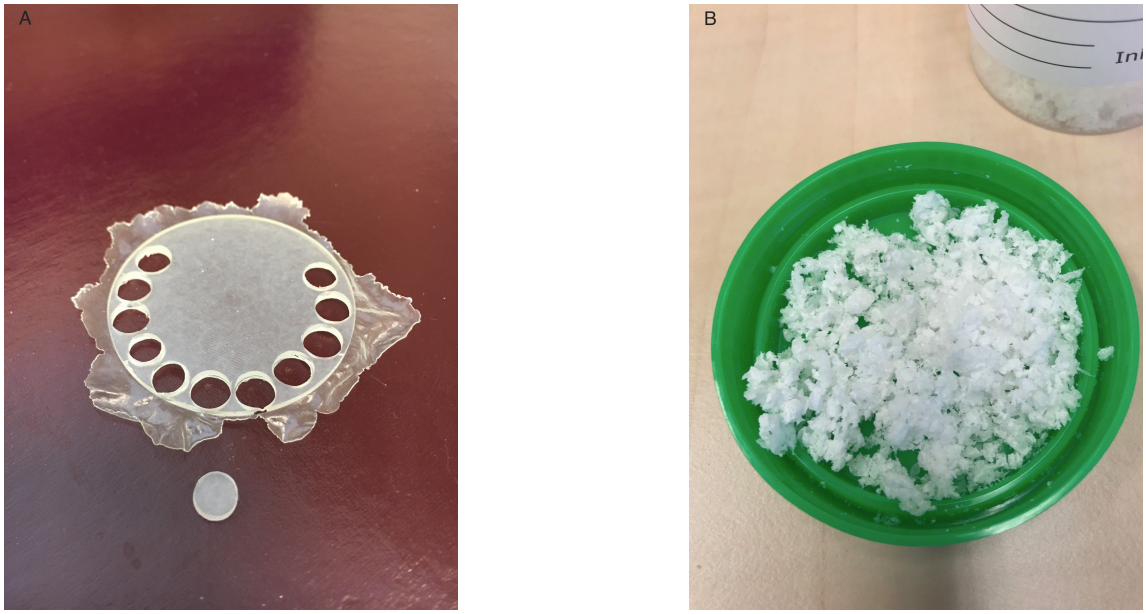

Figure 2: (a) Press molded PCUU disc delivered by Polyvation B.V. with smaller diameter (6 mm) punched sample. (b) Grains of PCUU delivered by Polyvation B.V. suitable for 3D printing purposes.

2.2 Cell harvest and culture methods

Three different cell types were used for our in vitro experiments; equine chondrocytes, ATDC5 cells and equine articular cartilage progenitor cells.

Equine chondrocytes

Equine chondrocytes were initially the cell type of choice for all in vitro tests as the elastomer part of the implant will be surrounded by equine cartilage in vivo as well. The attachment of these cells in vitro to the elastomer is therefore extremely important to predict in vivo outcomes. The equine chondrocytes used were previously isolated under sterile conditions from macroscopically healthy stifle joints of warmblood horses that were euthanised in the Department of Equine Sciences, Faculty of Veterinary Medicine (Utrecht University, the Netherlands). Two donors were used; EQ031, passage (P)0, sp 12-08-2015 and EQ033, P0, sp 13-08-2015. For isolation and culturing protocols, please see Appendix "Equine chondrocytes".

ATDC5 cells

As initial experiments showed poor attachment of the equine chondrocytes to the elastomer, and donor cells are precious, we decided to temporarily switch to the chondrogenic cell line ATDC5. This clonal cell line is isolated from the mouse teratocarcinoma stem cell line AT805 on the basis of chondrogenic potentials in the presence of insulin [21]. ATDC5 cells are known for their sequential transition of phenotype, quick attachment, and ease of culturing. They encompass chondrogenic differentiation from mesenchymal condensation to calcification [22]. Especially their excellent attachment properties and ease of culturing were reasons for selecting ATDC5 cells for some of our in vitro tests. The ATDC5 cells were taken from the liquid nitrogen storage and were in their P18 from 11-11-18. For culturing protocols, see Appendix "ATDC5 cells".

Equine articular cartilage progenitor cells

In the previous study by Korthagen et al. it was hypothesized that the thin layer of cartilage-like tissue on top of the implant was mainly formed from the laterally present native cartilage. It is becoming increasingly apparent that growth of articular cartilage is achieved from the articular surface. For such a mechanism to occur, a population of stem or progenitor cells must be present. Dowthwaite et al. have found that articular cartilage progenitor cells (ACPCs) are present and can be isolated from the surface zone using differential adhesion to fibronectin [23]. As these cells could be the cells initiating the overgrowth of the implant, they are valuable to investigate. Therefore, equine cartilage progenitors were used in our in vitro experiments too. For isolation and culturing protocols, please see Appendix "ACPC".

2.3 In vitro analysis assays

To generate results of our in vitro experiments, multiple analysis instruments were used.

MTT assay

The 3-[4, 5-dimethylthiazol-2-yl]-2, 5 diphenyl tetrazolium bromide (MTT) assay is based on the conversion of MTT into formazan crystals by living cells, which determines mitochondrial (metabolic) activity. As for most cells the total mitochondrial activity is related to the number of viable cells, this assay is broadly used to measure the in vitro cytotoxic effects of a condition presented to the cells [24]. The MTT assay is therefore highly suitable to test the influence of our PCUU samples to targeted cell lines or primary donor cells. The results of the MTT assay can be read out by a microplate reader. In our experiments the VersaMax microplate reader for 96-well format (Molecular Devices, USA) was used. For the protocol used, please see Appendix "MTT assay".

DNA Qubit assay

One of the most frequently used methods to perform a DNA assay is the Qubit system. The Qubit system is based on the gold standard of DNA assay, PicoGreen [25]. This assay is highly functional to determine the relative amount of cells that have attached to the bottom of the well plate versus the amount that attached to the elastomer. Before

the start of the assay, cell lysis is perfomed by adding Triton (Sigma-Aldrich, USA), releasing the cell's dsDNA. Fluorescent dye is added to measure the concentration of this dsDNA and afterwards read out by the Qubit 2.0 Fluorometer (Invitrogen, USA). The quantity of dsDNA/ml gives you data on the relative amount of cells that were present in a solution. For further details and the protocol, please see Appendix "DNA Qubit assay".

Wettability test

As discussed before, cells generally prefer to attach to hydrophilic rather than hydrophobic surfaces. To test the wettability of a solid material a test based on the contact angle (CA) between a liquid droplet and the material's surface can be performed, Figure 3a. The contact angle determines the wetting properties of the material. The smaller the contact angles, the more hydrophilic the material is, the larger the contact angle, the more hydrophobic. The PCUU's contact angle was determined by performing a sessile droplet test on the OCA 15EC (DataPhysics Instruments, Germany). Images from the machine were derived and analysed with the provided software, Figure 3b. For details on the wettability tests and the protocol. please see Appendix "Wettability test".

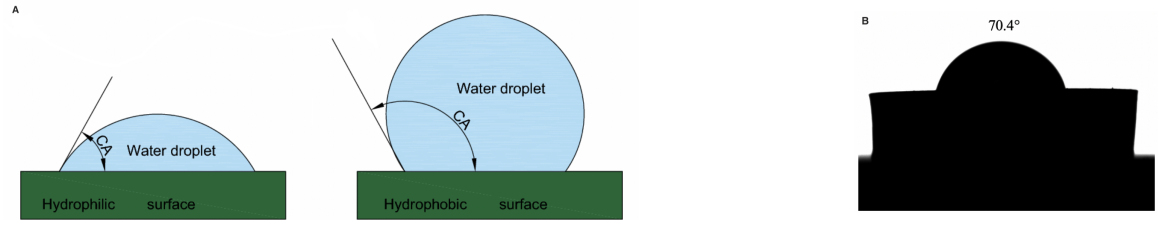

Figure 3: (a) Example of how to measure the contact angle of a water droplet on a hydrophilic and hydrophobic material [26]. (b) Wettability test of M927 PCUU performed by the OCA 15EC.

2.4 Elastomer modifications for cell adherence

As discussed, the major goal of this study is to adhere and anchor a layer of cartilage-like tissue to the elastomer. The initial experiments made it apparent that the equine chondrocytes had trouble adhering to the elastomer. As a result, multiple strategies were applied to improve the adherence properties of the elastomer. From a regulatory point of view it was not preferable to add any peptides or other add-ons to the material as it would make clinical approval more complex. Therefore, etching, punching holes, and 3D printing were analysed as potential solutions.

Etching

The first strategy was to perform surface treatments on the elastomer by etching. Surface treatments are a well known approach to change cell behaviour as surface treatments can alter the surface topography [27]. Kay et al. for instance showed that certain topographic nanostructures enhance chondrocyte adhesion [28]. Besides enhanced adhesion, Joergensen et al. showed that microstructures caused by etching showed dramatic increase of chondrocyte proliferation rate as well [29]. Another benefit of etching is the potential change in wettability [30]. It is widely accepted that cells prefer to attach to hydrophilic rather than hydrophobic surfaces [31].

Four different etching treatments were tried to improve chondrocyte attachment. Although the hydrophilicity did improve on 3/4 treatments, no treatment significantly improved cell attachment results compared to the untreated sample and the strategy was terminated. Therefore, etching will not be included in the experiment section. Please see the Appendix "Surface treatments" for the material and methods, and results of these experiments.

Punched holes

Besides compressive forces, articular cartilage experiences shear forces as well. The neo-tissue layer on top of the implant should therefore be securely anchored to the elastomer resisting detachment by shear forces. Tissue ingrowth into punched holes in the elastomer could provide this resistance.

Literature was consulted to determine the different hole diameters used for our experiments and how to align them. Seong et al. found that aligned pores exhibit superior mechanical strength to randomly oriented pores [32]. Since we initially desired a porous material without compromising the mechanical strength too much, aligned pores seemed the best option. Seong et al. also studied optimal cartilage regeneration with different diameter holes. A 270 μm hole diameter was found to be optimal. According to Lien et al. the optimal pore diameter for the proliferation and extracellular matrix (ECM) production of chondrocytes lies between 250 μm and 500 μm [33]. Another study by Jia et al. found that cell proliferation in scaffolds with bigger pore sizes (450 μm) was higher than that in constructs with smaller (200 μm) pore sizes [14]. These results are in line with previous reports by Levingstone et al. [34].

Taken the above into account, we decided to focus on hole diameters between 300-500 μm. Initially these holes were created by drilling, however, due to the viscoelastic properties of the elastomer this was extremely difficult and all holes smaller than 500 μm did not remain open after removal of the drill. Alternatively, core punches were used. Reusable WellTech rapid-core punches of 350 μm, 500 μm and 1000 μm (World Precision Instruments, USA) were used to create functional holes. These diameter punches were chosen as 350 μm and 500 μm punches were the two smallest diameters available on the market and were therefore closest to our aim diameter. Besides that, a larger control group of 1000 μm was added to compare to literature findings.

Due to the elastic behaviour of the elastomer, the punched hole diameter did not match the exact diameter of the punch. At the top surface where the punch initially makes contact with the elastomer the diameter is identical to the punch diameter as little force is needed for the razor sharp cutting edge to penetrate the surface. However, to penetrate the entire elastomer, significant force was needed causing the wall of the punched hole to recuperate, leaving a diameter smaller than the diameter of the punch. This can clearly be seen in Figure 4. Therefore, the "actual" diameter of the hole had to be determined.

To calculate the actual diameter of the holes, all three diameter holes were made in triplicate in an elastomer sample and cut sagitally right through the middle of the holes, exposing a view of the entire length of the shaft. Microscopical images of the shaft were taken with the Olympus IX53 (Olympus scientific Solutions, USA) at 4x magnification. With the help of the computer program Fiji ImageJ ^{TM}, the images were analysed and the initial diameter (top of the elastomer) and actual diameter (middle of shaft) were compared based on pixel diameter. As the initial diameter was known (350, 500 and 1000 μm), the actual diameter could easily be determined by dividing the actual diameter pixels by the initial diameter pixels, then multiplied by the initial diameter in μm. By doing so, the actual diameters showed to be 188 μm (350 μm), 319 μm (500 μm), and 741 μm (1000 μm), Figure 4,

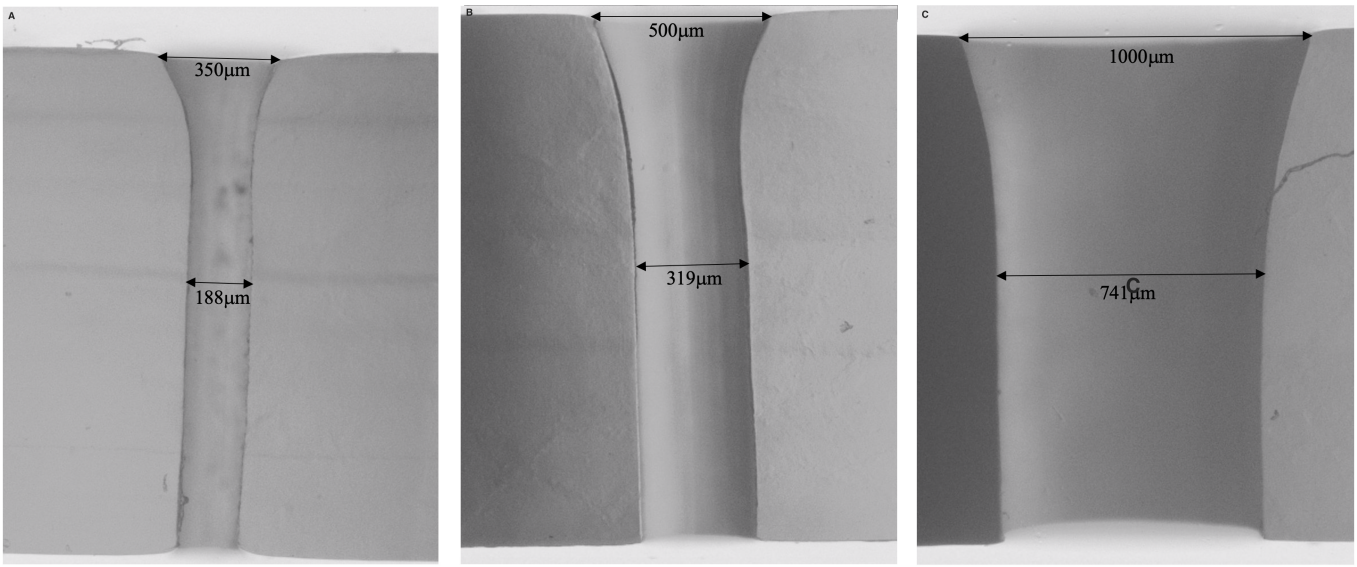

Figure 4: Cross section of the initial and actual diameter of the 350 μm (a), 500 μm (b), and 1000 μm (c) punched holes calculated with ImageJ.

3D printing

Besides punching holes, 3D printing is an excellent strategy for tissue ingrowth and adhesion. 3D printing provides the opportunity of creating a custom made porous structure that can provide optimal pore properties for cartilage ingrowth and regeneration. Porous scaffolds and implants have already shown great potential and results in cartilage tissue engineering for many years [35][36]. The main benefit of a 3D porous environment versus aligned holes is the possibility of creating interconnected pores which substantially improves nutrient flow and enhances cellular adhesion and migration [37]. Besides that, grown-in tissue exhibits greater resistance against forces in all directions compared to punched holes as the 3D printed porous environment can enclose the tissue in all dimensions.

The most common methods for polymer printing are based on melting the polymer before extrusion or by sintering polymer particles together [38]. Unfortunately, our PCUU elastomer does not allow this as the hardblock component of the PCUU degenerates (220 °C) before reaching the melting temperature (Tm= 227 °C). Solution based printing therefore remained the only option within the facilities of our lab. Solution based printing works on the principle of dissolving a material in a closed environment, until a homogeneous viscous substance is created. This viscous substance is then transferred into a cartridge which can be used for extrusion based printing. After printing, the solvent evaporates quickly leaving only the original material to form a 3D construct. Due to the inertness of our elastomer in combination with the need for a quick evaporative solvent, few solvents were suitable for our purpose. On advice from the manufacturing company Polyvation B.V. a mix of trifluoroacetic acid (TFA) and dichloromethane (DCM) was used. Polyvation B.V. uses this mix of solvents themselves for determining the intrinsic viscosity of the PCUU at 1 volume% TFA in DCM. DCM itself is not potent enough to dissolve the PCUU, the TFA component is. However, during optimizing the material to solvent ratio, it became apparent that a larger percentage of TFA to DCM resulted in greater gas bubble formation after printing due to the evaporation of the solvent. These trapped evaporated solvent bubbles are undesirable as they potentially contain toxic gasses harmful to cells. Another contributing factor to the number and volume of the gas bubbles is the PCUU weight to solvent volume ratio. The more PCUU/ml solvent was used, the less bubbles appeared after printing. Up to a certain maximum, the more % TFA to DCM is used, the more PCUU can be dissolved per ml. Altogether, there is a trade-off between the solvents % TFA to DCM and the mg/ml PCUU dissolved in this solvent. The final ratio used was 180 mg PCUU/ml of 5 volume % TFA in DCM. For details of this optimization process, please see Appendix "3D print optimization".

3D printing was performed with the 3D Discovery ^{TM}(RegenHU, Switzerland), Figure 5. G-codes for the constructs were handwritten and an interfacial engineered architecture that creates porosity between the lattices was used. A microscopical side view image of an interfacially 32-layered M927 PCUU 3D print can be seen in Figure 6a. A simplified animated version of an interfacial architecture can be seen in Figure 6b. This architecture was chosen as it creates both top and side porosity. It therefore allows for improved ingrowth and adherence potential compared to solid side walls. The rectangular infill pattern was chosen as it is simplest to print and we initially had severe problems with the printability of the PCUU solvent. For printing the M727 and M927 PCUU, the following parameters were used: cartridge: 3ml (Nordson EFD, USA) nozzle: 27G transparent (Nordson EFD, USA), printspeed: 15 mm/s, pressure: 90 kPa, layer height: 0.03 mm. Directly after printing the constructs were placed in a vacuum machine at 600 mbar for 1 hour to minimize the number of trapped gas bubbles. Afterwards a washing protocol was followed prior to any cell culture, Appendix "3D print wash protocol".

2.5 Mechanical tests

Mechanical tests were performed to analyse the differences in mechanical properties between the elastomers and native cartilage. The aim of the elastomer component of the implant is to mimic the mechanical properties of native articular cartilage. Compressive stress relaxation properties of the elastomer are one of the mechanical aspects that is desired to be similar to the native cartilage and is therefore investigated. Stress relaxation after a step strain is the fundamental method in which the relaxation modulus (G(t)) is defined [40]. For this test, a sample is suddenly deformed at a certain strain rate to a given strain (ε_0), and the resulting stress is measured as a function of time ($\sigma(t)$). The stress relaxation modulus can then be determined using the following equation (1).

$$G(t) = \frac{\sigma(t)}{\varepsilon_0} \tag{1}$$

Figure 5: RegenHU 3D Discovery bioprinter (RegenHU, Switzerland)

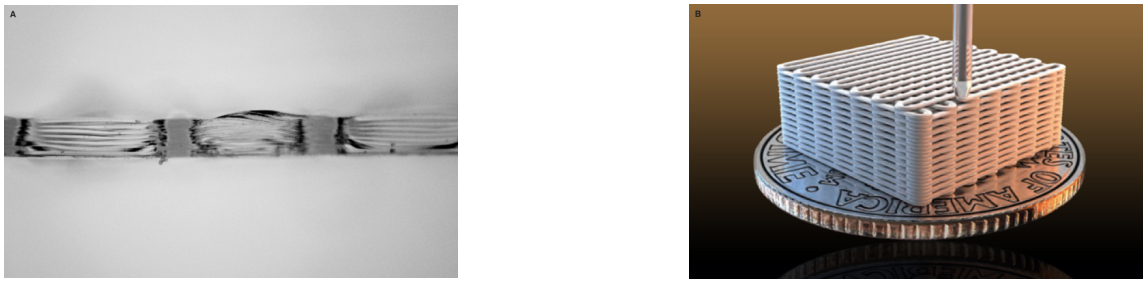

Figure 6: (a) Microscopic side view of an interfacially 32-layered porous M927 PCUU 3D printed construct. Image derived with the Olympus SZ61 (Olympus Scientific Solutions, USA). (b) Animated interfacially layered porous 3D printed construct similar to our 3D printed construct [39].

By keeping the strain rate fixed for an infinite amount of time, the resulting stress should eventually reach equilibrium. At this point were the $\Delta\ \sigma$ reaches 0, the compressive equilibrium modulus of a material can be determined by the same formula (1). This modulus is a measurement of the intrinsic stiffness of a material in equilibrium.

Stress relaxation tests were performed using a Dynamic Mechanical Analysis (DMA) Q800 machine (TA instruments, USA), Figure 7a. The DMA machine consists of a upper clamp assy and a lower driveshaft were the sample is clamped in between, Figure 7b. During compression the inner mechanism measures the parameters necessary to determine the mechanical properties of the sample. The test is classified as an unconfined compressive test.

Previously, stress relaxation tests were done by Korthagen et al. as well. It was decided to use the same parameters to generate our data as the parameters were thought to be valid and made comparison of results more reliable. The only difference is that we added a preload of -0.5% strain for 60 s to ensure tight clamping of the PCUU between the clamp assy and the driveshaft of the DMA machine before advancing to the actual stress relaxation test as this was advised by Olvera et al. [42]. After applying preload, the specimen was compressed with a ramp strain with a strain rate of -30%/min up to a strain of -5.5% ($\Delta\ \varepsilon$ of 5% compared to preload) which remained constant for 1800 s, Table 2. All tests were done in triplicate. During the tests, static force, displacement, strain and stress were recorded and afterwards, stress relaxation curves were obtained from the data, Figure 8. Furthermore, the stress relaxation modulus G(t) at the onset of the stress relaxation (G(0)) and 1800 s after the onset (G(1800)) were determined by using equation 1. G(0) was determined at the peak of the stress relaxation curve where the stress reached a maximum. G(1800) was determined from the last data points of the test, approaching equilibrium. We therefore consider the G(1800) as a compressive equilibrium modulus making it able to compare to cartilage moduli derived from literature. Mechanical data of cartilage had to be extracted from literature as the unconfined nature of the DMA test led to dried out samples of equine donor cartilage during testing, resulting in unreliable results that were excluded from this report.

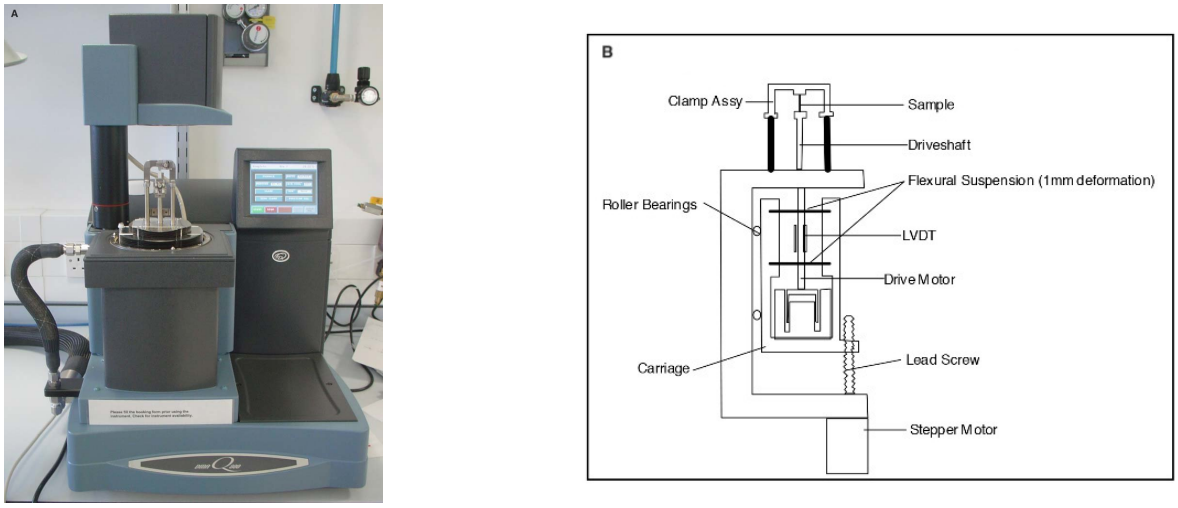

Figure 7: (a) Dynamic Mechanical Analysis (DMA) Q800 machine (TA instruments, USA). (b) Close-up of DMA mechanism [41]

Table 2: Parameters set on the DMA machine, used for all mechanical tests.

Parameter	**Value**
Preload	
Initital strain	-0.5% (60 s)
Loading	
Ramp strain	-30%/min to -5.5%
Isothermal strain	-5.5% (1800 s)

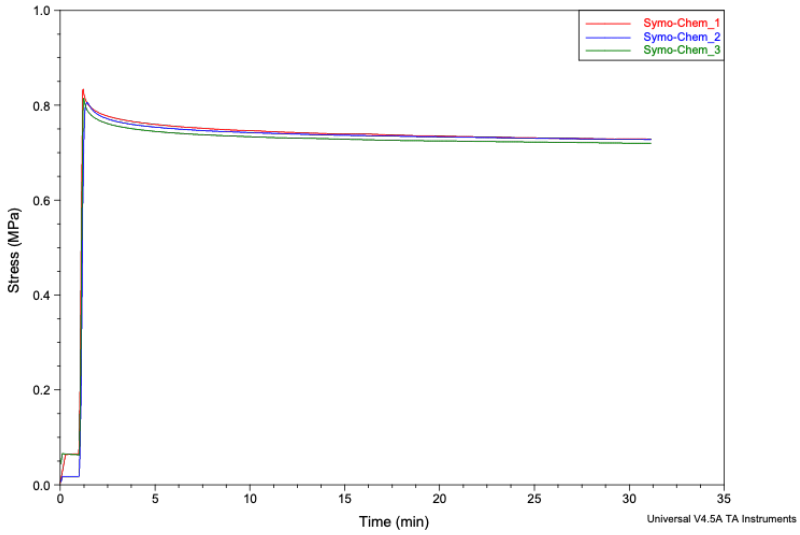

Figure 8: Stress relaxation curves of the Symo-Chem B.V. material, performed with the DMA Q800 machine using settings described in Table 2.

2.6 Statistical analysis and error measurement

All our tests results contained continuous data since it can be measured on a continuum or scale. Besides that, we always performed comparisons between different groups (PCUU vs. negative/positive control, one type of PCUU vs. another type etc.) meaning that we have unpaired data. To determine what type of statistical test to carry out, we should decide whether our data is normal or non-normal distributed. However, this decision is not black and white as it is dependent on many factors [43]. Sample size has a significant effect on sample distribution. It is often observed that small sample sizes, like our usual n=3, results in non-normal distribution. This is a results of inadequate estimation of the dispersion of the data, making it unknown if the frequency distribution will results in a normal curve [44]. However, some argue that theoretical considerations can help to make a decision too. If the outcome measures are known to be normally distributed, it can be assumed that the outcome data is normally distributed too. For instance, the MTT and the DNA Qubit assay outcomes always fall within a certain range and normality could be assumed here. Besides that, DMA and wettability experiments were repeatedly performed with different PCUU's in triplicate with all very concentrated data, and normal distribution of these tests are described in literature [45] [46]. It is therefore decided to regard our data as normal distributed. Conclusively, an unpaired t-test will be carried out between two groups and when more groups will be compared, an one way ANOVA will be performed, statistical significant difference is achieved when $p<0.05$.

With large normal distributed data, graphs and tables are normally presented with mean values and standard deviations of the larger data. This is done as it provides the viewer with an immediate impression of the data and the dispersion of it. Moreover, it decreases the data points to watch. With our triplicate tests this mean value and standard deviation does not dramatically decrease our data points and can be unreliable [47]. Accordingly, it is decided to not display standard deviations in our graphs and tables. Instead, all individual data points will be displayed as dots of a slightly lighter coloured version of the mean value bar of the outcome data. In this way, viewers still gets an immediately impression of the data with the opportunity to examine all data point as well.

To minimize the chance of any measuring errors, all analysis machines that could and were allowed to be calibrated (DNA Qubit, DMA Q800), were calibrated before use. Besides that, negative (and positive) control for the DNA Qubit and the MTT assays were employed to ensure optimal accuracy in results.

3 Experiments and results

3.1 Experiment 1: ATDC5 attachment to PCUU

Materials and methods

The goal of this experiment was to test how well ATDC5 cells attached to three different types of PCUU; M726, M727 and M927. These three PCUU samples were chosen as each of them were produced with unique production methods, see Table 1. The results should conclude whether or not these different production methods significantly altered the cell attachment properties of the PCUU. Tests were performed with $\oslash$ 6 mm punched samples sterilized with UV for 30 minutes on both sides at 39.5 mJ/cm^2 by the CL-1000 UV crosslinker (Ultraviolet Products Inc., UK). PCUU samples were individually placed in a well in a 48 wells cell culture plate (Greiner bio-one, Cellstar 48 Well Cell Culture Plate, Cat.-No. 677-180) and 500 μL, 400.000 cells/ml medium was added before incubating for 24 hours at 37 °C with 5% CO_2 in an incubator. A negative control well only containing the cells/medium suspension was included. Afterwards, the PCUU samples were carefully transferred to a fresh well and the DNA Qubit protocol was followed, Appendix "DNA Qubit assay". All tests were done in triplicate in the same cell culture plate.

Results

Results of experiment 1 can be found in Figure 9a. The graph shows a representation of the proportion of cells that adhered to the surface of the well plate and the proportion that adhered to the PCUU sample. The larger the proportion of cells attached to the construct, the better the cell adherence properties of the PCUU are. These values are also compared to the control group, not containing a construct, to ensure no disadvantageous effects to the cells are caused by the constructs. Regarding the total ng DNA/mL per well of the PCUU samples (no construct

+ construct) vs. the control group, no significant differences were found using the one-way ANOVA (p=0.106), meaning no significant effect on cell growth was experienced by the presence of the PCUU.

To determine whether the number of attached cells on the PCUU samples differed significantly, the one-way ANOVA test was again performed. When comparing all groups together through the one-way ANOVA, a slight statistical significant difference between groups was found (p=0.048). However, when determining which group differed significantly by comparing groups individually to each other with the one-way ANOVA multiple comparison, using the Tukey's multiple comparisons test, no significant difference was found. Although, M727 vs. M927 and M726 vs. M927 approached significant difference p=0.057, and p=0.087 respectively, indicating superior cell binding properties of the M927. This change in significant difference is due to the correction for multiple comparisons using statistical hypothesis testing. This can make the difference between just significant (p=0.048) and almost significant (p=0.057). Conclusively, no significant difference between groups was found.

The ratio between how many cells adhered to the surface of the well plate (no construct) and to the construct (construct) is very dependent on the size of the well plate and the PCUU sample. Both provide a certain surface area to adhere on. For the 48 wells plate, the bottom surface area is 1.000 cm^2 [48]. The surface area of the $\oslash$ 6 mm PCUU sample from top view is $\pi * 0.3^2 = 0.283\, cm^2$. However, the PCUU sample has more surface area when regarding it as 3D. For our calculation we assume that cells can attach anywhere on the construct and anywhere on the well plate. Then the total surface area of the 3D construct is $topsurface + bottomsurface + sidesurface$. The sides create a surface area of $(2 * \pi * 0.3) * 0.143$ $(perimeter * height) = 0.270\, cm^2$, creating a total PCUU surface area of $2 * 0.283 + 0.270 = 0.836\, cm^2$. Making the PCUU surface area 45.5 % of the total potential surface area to adhere on per well. If the cells would have no preference on where to adhere on, this should be the percentile ratio between the ng DNA/mL "construct" and "no construct". This was not reached in any of the PCUU samples in this experiment (M927 was best with 37.5 %) Figure 9.

3.2 Experiment 2: ACPC attachment to PCUU

Materials and methods

The goal of this experiment was to test how well equine articular cartilage progenitor cells attached to the M927 PCUU. The donor used was EQ 19.002 p0. Besides different PCUU's, cells and culture medium, all methods were identical to experiment 1.

Results

Analyzing the results in Figure 9b, a large difference between the total ng DNA/mL of the M927 and the control can be observed. This observation is confirmed by performing a t-test with solid statistical significant difference (p=0.00002). Besides that, on average, 42.9 % of the cells attached to the PCUU which is close to the 45.5 % of no preference.

3.3 Experiment 3: Equine chondrocyte attachment to PCUU

Materials and methods

The goal of this experiment was to test how well equine chondrocytes attached to the M927 PCUU compared to the M524 PCUU as we initially had trouble attaching equine chondrocytes to the M524. During the initial M524 test, different culture methods were used than the ones described in experiment 1 and 2. We previously used 96 well plates vs. the current 48 well plates, ethanol sterilization vs. UV sterilization, 1 week vs. 24 hours, and different donors (EQ031, sp 12-08-2015 vs. EQ033, P0, sp 13-08-2015). It was investigated whether these different culture methods were the cause of the poor adherence or that equine chondrocytes simply did not enjoy attaching to the M524 or M927. The donor used was EQ033, P0, sp 13-08-2015. Besides different PCUU's, cells and culture medium, all methods were identical to experiment 1 and 2.

Results

When evaluating the total amount of equine chondrocytes attached with the M524 and M927 compared to the control, we can again observed a large difference, Figure 9c. The one-way ANOVA test confirm this with reliable statistical significant difference (p=0.026). However, comparing the M524 to the M927, no statistical significant difference was found in total (p=0.997) and between adherence to construct (t-test, p=0.451). On average 37.9% (M524) and 42.4% (M927) of the total chondrocytes attached to the PCUU which is a proper indicator that equine chondrocytes do not avoid attaching to the PCUU as was found in early studies with the M524. Poor cell culture methods and/or cell donor should therefore be the cause of the previously poor adherence.

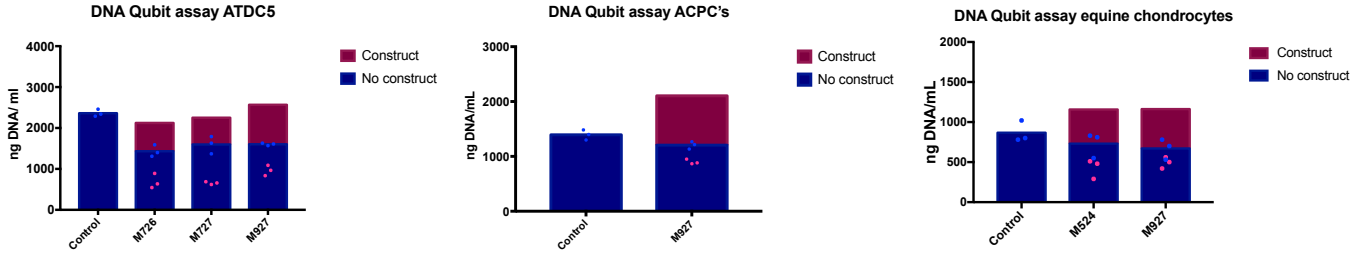

Figure 9: Results of experiment 1,2,3, displaying the ng DNA/mL detected in the control well and the different PCUU sample wells for ATDC-5 (exp1), ACPC's (exp2) and equine chondrocytes (exp3). PCUU bars show distinction between the proportion of cells adhered to the well plate (no construct) and the proportion adhered to the construct (construct).

3.4 Experiment 4: Wettability of PCUU

Materials and methods

In addition to the previous tests, a wettability test was performed with the M524, M726, M727, and M927 PCUU to investigate whether potential differences in cell attachment could be explained by difference in wettability. Besides that, it can be determined whether different production methods changed wetting behaviour.

Results

Although no official statistical significant differences were found between any attachment properties of the PCUU's, the M927 PCUU was approaching significant difference in experiment 1 versus the M727 (p=0.057). Many factors can change difference in cell attachment properties and wettability is an important one of them. Figure 10 shows the results of the wettability test performed. Absolutely no significant difference was found between any of the four PCUU's (p=0.938) concluding that wettability has had no factor in potential differences in cell attachment properties. Besides that, production methods did not interfere with wettability of the PCUU.

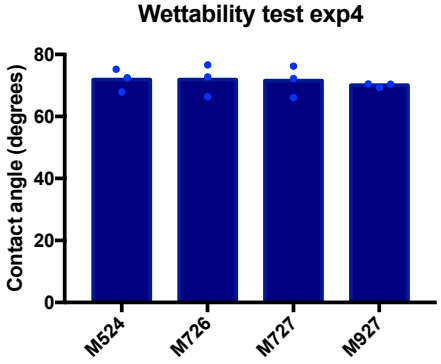

Figure 10: Wettability results of experiment 4, data derived from using the OCA 15EC.

3.5 Experiment 5: Optimal hole diameter

Materials and methods

The goal of this experiment was to determine the optimal hole diameter in M927 PCUU constructs for equine ACPC's to grow into. The three different diameter holes (actual diameters: 188 μm, 319 μm, 741 μm) discussed earlier were investigated. Each ⌀ 6 mm PCUU sample received 7 hand punched holes of the particular hole diameter investigated, Figure 11. All tests were done in triplicate. Cell culturing methods were identical to experiment 2, besides, culturing was done for 14 days instead of 24 hours, changing medium twice a week. All constructs were placed with their initial diameter facing up to identify differences in bottom-up growth in each sample after culturing. After 14 days of culturing, all samples were taken out of their well and carefully sagitally cut right through the middle of the holes using a microtome blade under a microscope. These cut samples were then transferred to a fresh well and stained with 4,6-diamidino-2-phenylindole (DAPI), see Appendix "DAPI protocol" for further details. Fluorescent images were taken with both the Leica SP8-X confocal microscope (Leica Microsystems, Germany) and the Olympus IX53. Both microscopes derive images from the bottom allowing the microscope to look into the shaft of the cut hole when constructs are flipped sideways generating useful images of the attached cells inside. Images were analysed using ImageJ and number of cells per surface area was determined.

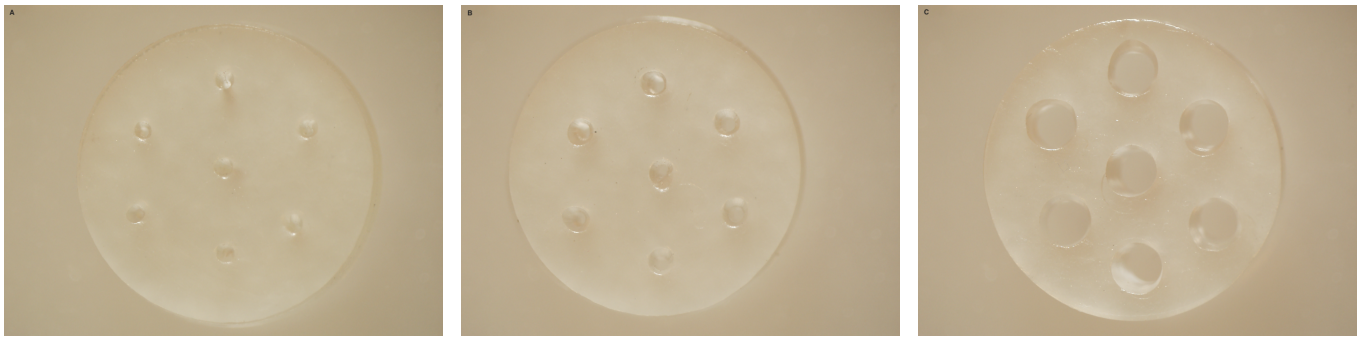

Figure 11: Top view close-up of ⌀ 6 mm M927 samples with 7 punched 350 μm (a), 500 μm (b), and 1000 μm holes (c). Image derived with Olympus SZ61.

Results

Microscopic fluorescence images after 14 days derived with the Olympus IX53 (2D) and Leica SP8-X confocal (3D) can be found in Figure 13, 14 and 15. ACPC's were found to adhere along the entire length of all diameter shafts. However, they did not fill any of the holes completely, they merely attached to the walls of the holes, Figure 14. The highest number of total cells can be found in the 741 μm shaft. However, the surface area for the cells to adhere on is far larger on the 741 μm hole compared to the other two. Therefore, the number of cells per surface area has to be calculated to determine the optimal hole diameter.

2D images derived with the Olympus IX53 were used to determine the cells per surface area with ImageJ software. A surface area of 188 μm x 1166 μm, 90 μm from the bottom, in the middle of the shaft was analyzed in all three diameter holes in triplicate, Figure 16. As ImageJ had trouble identifying individual cells when there were clustered, it was chosen to determine the percentage of the surface covered with cells. ImageJ is able to converse all the cell pixels to white and the background to black making it able to determine the percentage of white pixels versus black pixels in a certain area, hence, determining the percentage of cells coverage, Figure 16.

Since all three diameter holes have different arc lengths, the examined surface area is different for all three shafts. The percentage of cell coverage therefore needs to be adjusted to reflect the actual percentage of cells per surface area. To determine the arc length (a) of the analyzed surface area the following formula can be used (2). Where θ is the angle of the analyzed arc in degrees and r is the radius of the hole.

$$Arc\,length\,of\,circle\,(a) = \frac{\theta \pi r}{180} \tag{2}$$

θ is known for the 188 μm hole since it is analyzed in its full 180 degrees. However, For both the 319 μm and 741 μm holes, the θ is unknown. This can be calculated using the circle to arc correlation model in Figure 12. We use equation 3.

$$sin(\frac{\theta}{2}) = \frac{c/2}{r} \tag{3}$$

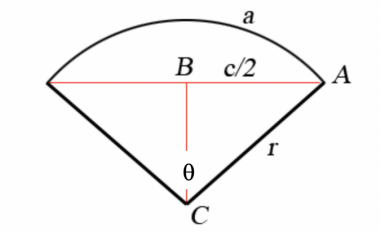

Figure 12: circle to arc length correlation model to determine the actual surface area for experiment 5 [49].

To calculate the total surface area, the arc length of the circle should then be multiplied by the length of the surface area analyzed which is the same for all diameters (1166 μm). The final surface area for the 188 μm = 0.344mm^2, 319 μm = 0.235mm^2, and 741 μm = 0.222mm^2. The adjusted percentage of cell coverage can be found in Figure 17. Both 319 μm and 741 μm performed significantly better than the 188 μm (p=0.009 and p=0.041). Nonetheless, no significant difference was found between 319 μm and 741 μm (p=0.446), although the highest mean score was achieved with the 319 μm holes.

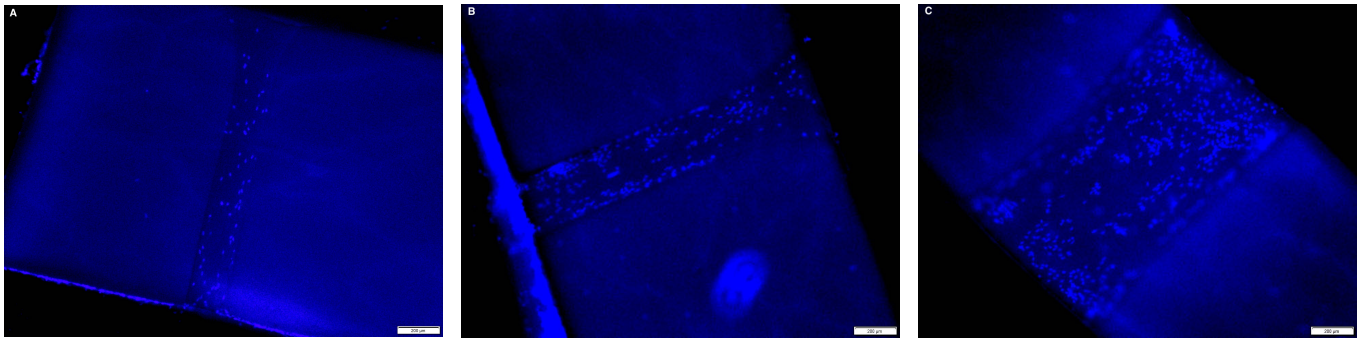

Figure 13: 2D microscopic side view of sagitally cut 188 μm (a), 319 μm (b), and 741 μm (c) shaft after 14 days of culturing. ACPC's stained with DAPI. Image derived with Olympus IX53.

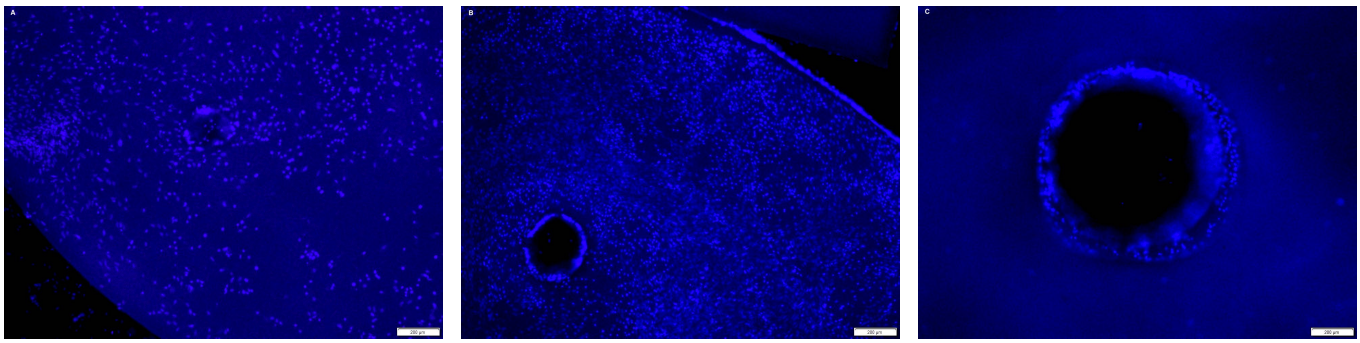

Figure 14: 2D microscopic bottom view of 188 μm (a), 319 μm (b), and 741 μm (c) holes after 14 days of culturing. ACPC's stained with DAPI. Image derived with Olympus IX53.

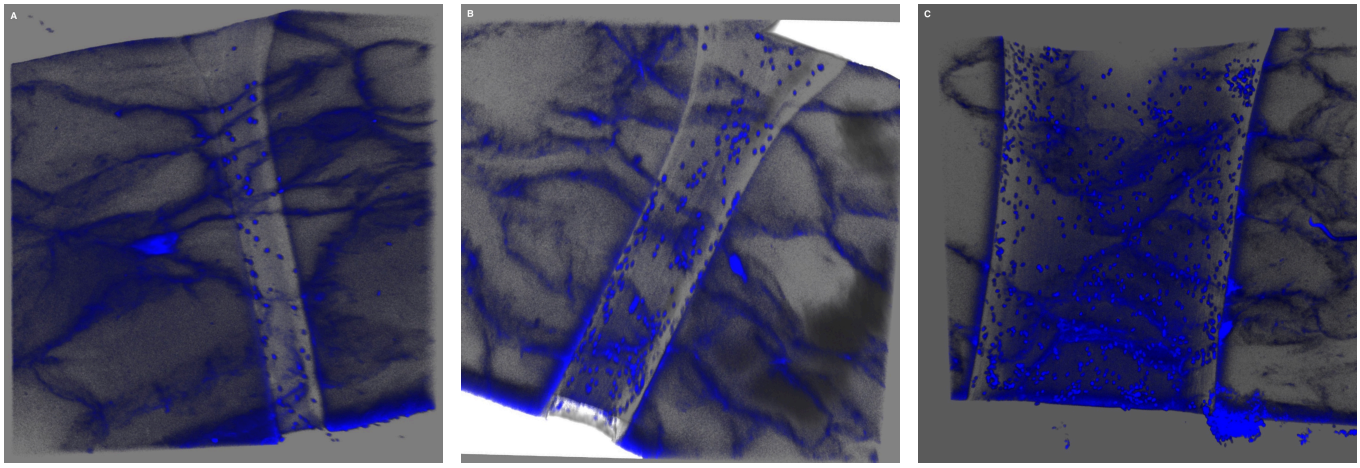

Figure 15: 3D microscopic side view of sagitally cut 188 µm (a), 319 µm (b), and 741 µm (c) shaft after 14 days of culturing. ACPC's stained with DAPI. Image derived with Leica SP8-X confocal.

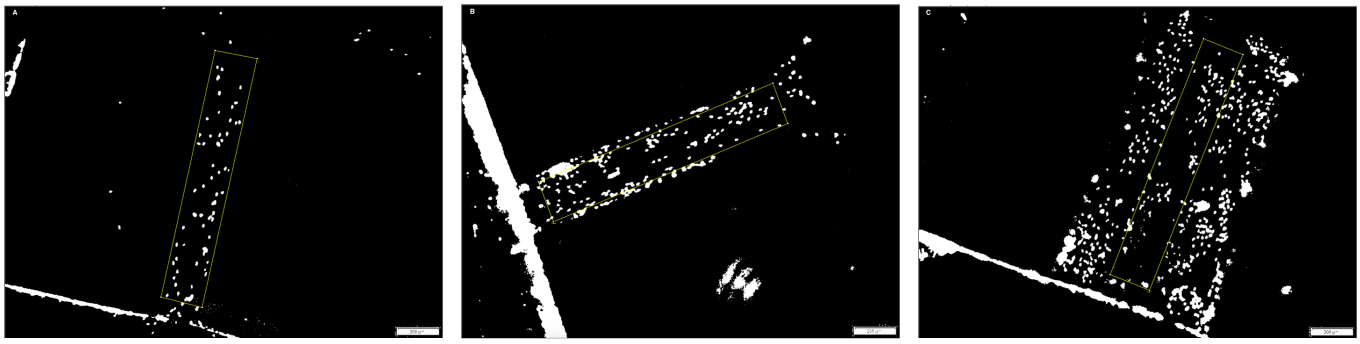

Figure 16: Surface area of 188 µm (a), 319 µm (b), and 741 µm (c) hole analyzed in ImageJ for cell count to determine optimal hole diameter.

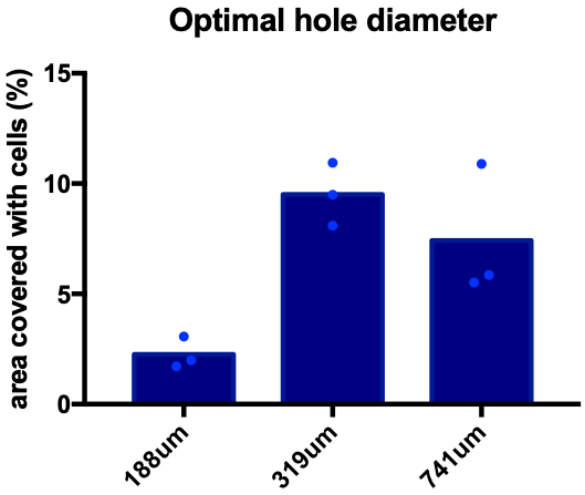

Figure 17: Results of experiment 5, showing the percentage of cell coverage in all three different diameter holes.

3.6 Experiment 6: Cytotoxicity of 3D printed constructs

Materials and methods

As the 3D printed PCUU constructs were printed from highly toxic solutions, it had to be determined whether this had any effect on cells. Accordingly, the goal of this experiment was to test the cytotoxicity of our 3D printed constructs on ATDC5 cells. The 3D printed constructs used were 6.5 x 6.5 mm containing 8 layers printed with M727 and M927 PCUU, Figure 18. Both a negative and a positive control were included in this experiment. The negative control consisted of a well just containing the cell/medium solution that was also added to the wells with constructs. The positive control was a handmade 3DP construct replica made out of press molded PCUU that already had proved in previous test not to evoke toxic response, Figure 18. This replica was made to mimic the 3DP construct's surface area, shape, thickness and weight. Firstly, the surface area and thickness of the 3DP was determined with a digital caliper. Next, a replica was made from the surplus press molded PCUU on the edge of the disc as it turned out to have very similar thickness to the 3DP, Figure 2. Next, it was calculated how the exact same surface area could be achieved by using 4, ⊘ 2mm punched holes in the replica as it mimics the shape of the 3DP. It was found that a rectangular of 5.2 x 5.2 mm was needed for this and subsequently this was cut out with a scalpel. Lastly, both constructs were weighted, 3DP= 2.1 mg, replica= 2,2 mg.

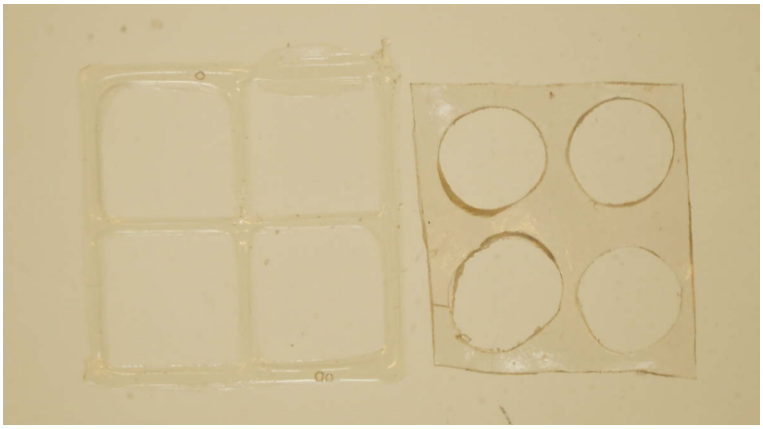

Figure 18: 3D printed construct (left) and 3DP replica (right), image derived with the Olympus SZ61.

Cells tests were performed by placing both the 3DP constructs and the 3DP replicas (UV sterilized) individually in a well of a 48 well culture plate and 500 μL, 400.000 cells/ml medium was added to them and the negative control wells before incubating for 7 days at 37 °C with 5% CO_2 in an incubator, replacing medium once at day 3. Afterwards a MTT assay was performed to derive the results. All tests were done in triplicate and as the plate reader was only compatible with 96-well plates, the volume of each 48-well was transferred to two 96-wells generating six results per test.

Results

The results of the MTT assay can be found in Figure 19. Better quality statistics compared to other experiments could be performed on these results as n=6. Using the one-way ANOVA multiple comparison test we can conclude that besides the M727 positive control, all other results exhibited significantly higher metabolic activity than the negative control. Besides that, no statistical significant difference was found between the 3D prints and the positives controls (M727 p=0.234, M927 p=0.374). Taking this into account, we can conclude that there is no cytotoxic effect on cells caused by either M727 or M927 3D printed constructs. In fact, ATDC5 cells in a well containing a 3D printed construct exhibit significantly higher metabolic activity than in wells without any construct.

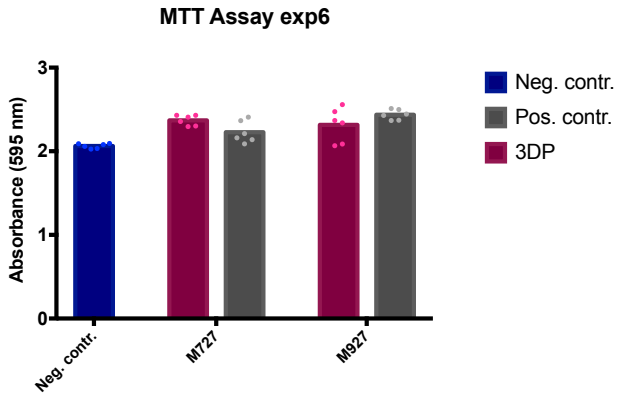

Figure 19: Results of experiment 6, showing the MTT absorbance (metabolic activity) of 3DP M727, M927 PCUU with a negative and positive control.

3.7 Experiment 7: Whole blood assay

Materials and methods

A whole blood assay is a reliable, reproducible, fast and feasible method to asses the immune response against a certain presented item or chemical [50]. In our case the whole blood assay was performed to asses the in vitro equine cellular immune response to press molded PCUU samples and 3DP PCUU samples. The intensity of the cytokine and chemokine response of IL-8, CCL-2 and TNF-α was measured with three different healthy equine blood donors with both negative and positive control. M927 PCUU samples with 500 μm holes, without holes, and 3D printed constructs were tested. For details on this test and protocol, please see Appendix "Whole blood assay".

Results

Results of the whole blood assay with TNF-α, CCL-2 and IL-8 can be found in 20. Permanent implants like ours should evoke the immune system least as possible to avoid in vivo infections and rejection. It is therefore desired to have results as close to the negative control as possible. Performing the one-way ANOVA multiple comparison test we can conclude that none of the plain, holes, or 3DP PCUU's in any of the cytokines/chemokines differed significantly compared to the negative control, while all did differ significantly to the positive control. Comparing to the negative control, closest p-value to significance difference is reached at the CCL-2 comparing the plain versus the negative control (p=0.461) which is still far from significant difference. Looking at the positive control, lowest significant difference is found between the plain and positive control in the TNF-α analysis (p=0.002), which is still a very convincing significant difference. We can therefore conclude that all three types of modified M927 PCUU do not, or hardly, evoke a immune response regarding these cytokines.

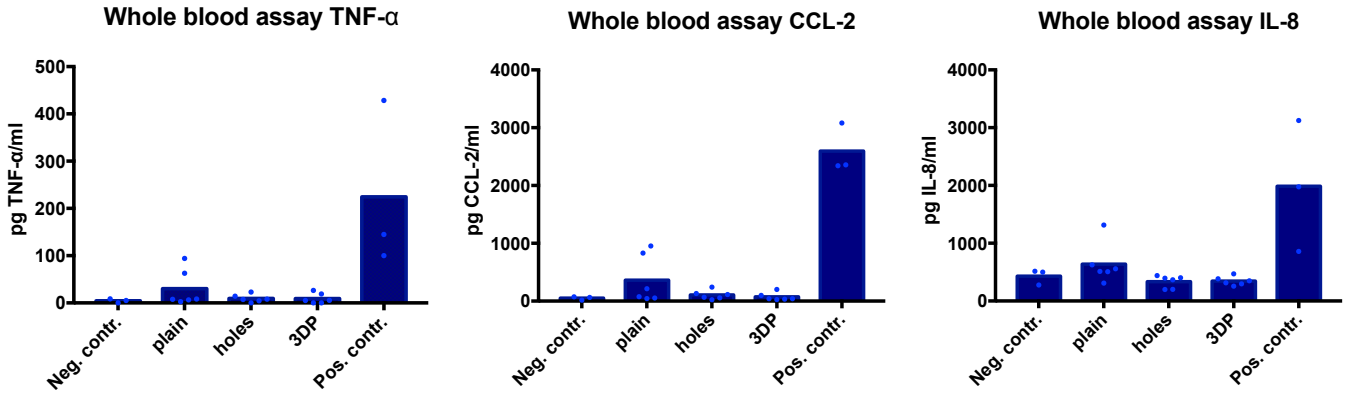

Figure 20: TNF-α, CCL-2, and IL-8 results of the whole blood assay with three different equine blood donors.

3.8 Experiment 8: Mechanical testing

Materials and methods

The goal of this experiment was to determine the stress relaxation moduli of three different elastomer samples; the previous elastomer produced by Symo-Chem B.V., M927 PCUU, and a 3D printed M927 PCUU sample. All tests were done in triplicate. The 3D printed sample was a 32 layered 3D print with interfacial layers, Figure 21. Details on the dimensions of the samples can be found in Table 3. Settings used on the DMA Q800 machine were identical to Table 2.

Table 3: Descriptions and dimensions of DMA tested elastomer samples

Test	Description	Dimensions
1	Symo-Chem	⌀ 3 x 2.93 mm
2	M927	⌀ 3 x 1.43 mm
3	3DP M927	□ 8 x 8 x 0.80 mm

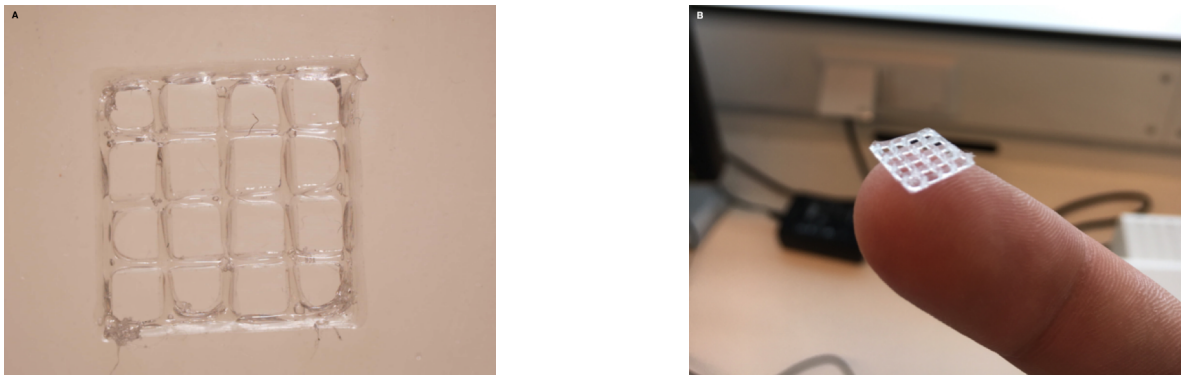

Figure 21: (a) Top view close-up of the M927 3D printed 32 layered construct. Image derived with Olympus SZ61. (b) Slanted view of the M927 3D printed 32 layered construct

Results

The results of the DMA tests performed with the Symo-Chem elastomer, M927, and 3DP M927 can be found in Figure 22. Stress relaxation moduli at G(1800) are considered as the compressive equilibrium modulus of the Symo-Chem, M927 and 3DP M927 and were found to be 13.19, 10.34 and 0.22 MPa respectively. All individual graphs like Figure 7 can be found in Appendix "DMA results". The goal of the elastomer part of the implant is to mimic the mechanical properties of native articular cartilage while providing an excellent porous structure to facilitate optimal cell ingrowth and adherence. According to Mow et al. human articular cartilage has an aggregate stress relaxation modulus of 0.76 MPa [51]. The aggregate stress relaxation modulus is a modulus derived from a compressive stress relaxation test and reflects the elastic modulus of the material at equilibrium when fluid has ceased flowing through it. It is therefore closest to our compressive equilibrium modulus as exact numbers on human articular cartilage equilibrium moduli were not found in literature.

Comparing the modulus of human cartilage to the M927 clearly shows that these are not similar. However, looking at the modulus of the 3D printed sample it can be observed that the modulus drops drastically making it even lower than that of cartilage, Figure 22. This provides opportunities as we desire a porous elastomer structure to enhance ingrowth and adherence of cells while maintaining proper mechanical properties. Two methods of porosity are used in this research; creating holes and 3D printing. For both of them it can be calculated what porosity and structure is necessary to achieve similar mechanical properties of articular cartilage. A compressive equilibrium modulus of 1.0 MPa is set as the goal for the porous constructs as it is in the range of native articular cartilage and still provides sufficient initial mechanical strength.

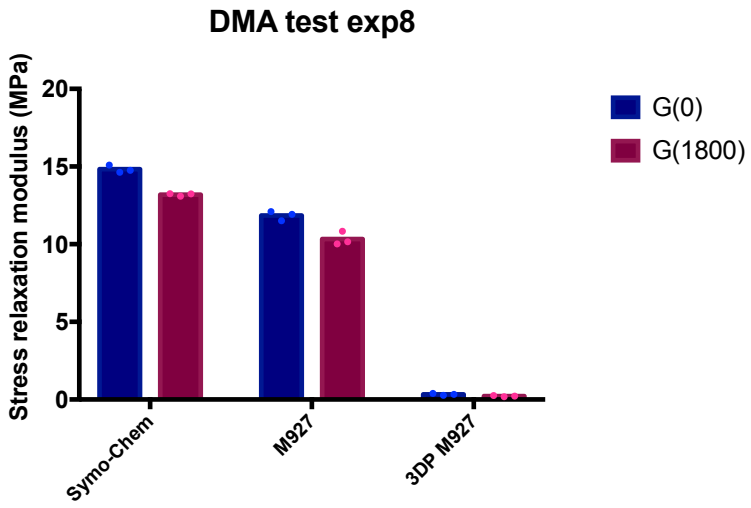

Figure 22: DMA results of experiment 8, onset stress relaxation modulus G(0) and compressive equilibrium modulus G(1800) are shown for the Symo-Chem elastomer, M927 PCUU and 3D printed construct of M927.

Punched hole mechanics

Considering equation 4 it can be noticed that stress (σ) is a linear function of force and surface area. Looking at equation 5 it can be seen that the stress relaxation modulus holds a linear relationship between stress and strain (ε). Combining the two makes it clear that the stress relaxation modulus holds a linear relationship with the surface area too. We can therefore calculate the needed surface area for the M927 to reach a modulus of 1.0 MPa. This can then be translated to the amount of punched holes necessary. As the highest mean score of cell coverage in experiment 5 was achieved with 319 μm holes we use this diameter to perform our calculations.

$$\sigma = \frac{force}{surface\,area} \tag{4}$$

$$G(t) = \frac{\sigma(t)}{\varepsilon_0} \tag{5}$$

The surface area of our solid 6 mm diameter construct is 28.274 mm^2 with a compressive equilibrium modulus of 10.34 MPa. To bring this modulus down to 1.00 MPa we should have a surface area of $\frac{1}{10.34} * 28.274 = 2.734\,mm^2$. Every punched 319 μm hole will diminish the surface area with 0.08 mm^2, which will demand a total number of holes of $\frac{28.274-2.734}{0.08} = 320\,holes$ while the maximum amount of 500 μm holes possible is 109 [52]. This diameter of 500 μm is used in the calculation as the initial diameter of entrance in the PCUU is 500 μm and this diameter will decide how many holes would fit next to each other. Even in the ideal situation where we could create perfect parallel holes (319 μm) this number would not be sufficient as we could achieve maximum 272 holes [52]. Creating 272 holes in the construct would result in a modulus of 2.38 MPa. Although it would be approaching the desired 1.0 MPa, it is concluded that punching hole is unfeasible in creating cartilage like mechanical properties. Therefore, we need to focus on 3D printing.

3D printing mechanics

The great benefit of 3D printing is that custom complex structures can be made with it. It also provides the possibility of creating highly porous constructs with interconnecting pores. Predicting the mechanical properties of these porous structures is dependent on many variables and not every structure is described in literature. We therefore decided to determine the 3D printed structure needed to reach a 1.0 MPa modulus in two ways. Firstly, we determine which shape and density a 3D print should posses to reach the desired modulus taking the solid PCUU's modulus as a reference. Secondly, we determine the density needed for the same architecture as the tested 3D print to reach the desired modulus, taking the 3D printed construct's modulus as a reference.

The most complete description of mechanical properties of different porous structures were found in the book "Cellular solids" by J. Gibson and F. Ashby [53]. Mechanical properties of many different structures are described, including honeycombs and squares. Therefore, these two porous structures will be discussed as potential 3D prints. Honeycombs are known for their low weight-to-stiffness ratio and outstanding energy absorption characteristics making them widely used in technological applications [54]. Furthermore, they are often used in 3D cell scaffolds as they provide excellent cell compatibility [55]. Besides that, creating a 3D print with honeycomb infill is very feasible using the RegenHU bioprinter together with the solved PCUU as honeycomb is one of the basic infill patterns. A square infill is most simple and already achieved to print with our PCUU and solvent mixture.

The equation for out of plane compression of square cell solids as described in the book by J. Gibson and F. Ashby can be found in equation 6. The equation for out of plane compression of honeycomb cell solids can be found in equation 7.

$$\frac{E_3}{E_s} = \left(\frac{2}{cos\alpha(1+sin\alpha)}\right)\frac{t}{l} = \frac{\rho}{\rho_s} \tag{6}$$

$$\frac{E_3}{E_s} = \left(\frac{\frac{h}{l}+2}{2(\frac{h}{l}+sin\alpha)cos\alpha}\right)\frac{t}{l} = \frac{\rho}{\rho_s} \tag{7}$$

E_3= elastic modulus (stress relaxation modulus) of 3D printed construct (MPa)

E_s= elastic modulus (stress relaxation modulus) of solid M927 PCUU (MPa)

α = the angle between two inclined members of the cellular structure (degrees)

t= wall thickness (mm)

l= length of the inclined members of the cellular structure (mm)

ρ_s= density of solid M927 PCUU (set as 1)

ρ= density of 3D printed construct (relative to ρ_s)

h= height of the inclined members of the cellular structure (mm)

For both the honeycomb and rectangular infill we can determine the necessary 3DP density to reach the desired modulus. Since E_3=1.00 MPa, E_s= 10.34 MPa and we set ρ_s=1.00 we can simply calculating the ρ using formula 6 or 7, ρ=0.085. Now we can determine the length of the inclined member of the square structure (l). In squares α=0 °and the optimal wall thickness (t) achieved in any of our 3D prints was measured to be 0.15 mm, these values are taken into calculations. Filling in these values in equation 6 we can calculate the length of the inclined members of the square, which is l=3.55mm. Next, we can determine the length of the inclined member of the honeycomb structure (l). Most often in 3D printing a hexagonal infill is used which is a honeycomb with the exact same height and length. In hexagons the α= 30 °. By filling in these values into equation 7 we can calculate the length of the inclined members of the hexagons, which was computed to be l=1.79mm. Both lengths of the inclined members of the square and hexagon would be very large compared to our optimal hole diameter to achieve our goal. Based on these calculations, it has to be concluded that solid wall 3D printing in squares or hexagons in unfeasible to reach our combined goal of a 1.0 MPa modulus while creating porosity in the range of desired pore size.

Lastly, we determine the structural properties of a 3D print with the same architecture we used in our 3D print experiments. The sample used in the DMA test can be seen in Figure 21 and its architecture can be seen in Figure 6. The main difference between this print and the described prints in the previous calculations is that this print does not have solid walls, it has interfacial layers creating side porosity. This will inevitable result in lower mechanical compressive resistance. The 3D printed construct used in our DMA tests had a length of inclined members (l) of 2.0 mm, wall thickness (t) of 0.25 mm and a compressive equilibirium modulus (G(1800)) of 0.33 MPa. Unfortunately, no equation or description of this particular architecture was found in literature. However, from equation 6 and 7 we know that density and elastic modulus have a linear relationship. This relationship is also applied for the following calculations.

For the modulus to increase from 0.33 MPa to 1.00 MPa, we have to increase the ρ three times. This would lead to a reduction of the length of in the inclined member from l= 2.00 mm to l= 0.67 mm. By optimizing the wall thickness from the current t= 0.25 mm to our finest wall thickness achieved of t= 0.15 mm, this would lead to a further reduction of the "l" by 40%. All together, this would generate a length of the inclined members of l= 0.40 mm. This length combined with the wall thickness of t= 0.15 mm would results in a pore size of 0.25 mm. This is well within our range of best performing pore sizes (319-741 μm). Conclusively, 3D printing with interfacial layer architecture is feasible in achieving our goals of mimicking the mechanical properties of cartilage while creating optimal pore sizes for cell ingrowth and adherence.

4 Discussion

Osteochondral repair remains a great challenge in both humans and animals, especially in large animals such as the horse. Given the complex hierarchical structure of the osteochondral tissue, there are many key challenges to be overcome. Common issues include insufficient mechanical properties of scaffolds, step formation at the interface with native tissue and inadequate integration with the surrounding tissue [19]. In general, no long term restoration of functionality has been achieved [9]. This study aimed to elaborate on the work of Korthagen et al. [19] who encountered obstacles in their in vivo studies as well. Especially connecting the covering cartilage tissue to the elastomer part of the implant was found to be problematic. Therefore, this study focused on improving the elastomer part of a PEKK and poly-carbonate-urea-urethane implant in order to improve cell binding properties and to optimize the elastomer's mechanical properties tot mimic native articular cartilage. In vitro tests were performed in preparation for future equine in vivo trials.

One of the main differences between this research and the research by Korthagen et al. is the different source and production method of the elastomer. The current producer Polyvation B.V. had to reinvent the wheel on the elastomer production which SyMO-Chem already had done. Besides that, this production process had to be optimized. Accordingly, our elastomer material is different from that of Korthagen et al. making all in vitro experiments done by Korthagen et al. obsolete for our research. We can therefore conclude this is rather a new implant based on previous findings than a modified version of Korthagen et al's. Furthermore, new batches of PCUU made experiments with earlier batches obsolete too. The final M927 batch is therefore decisive on the performance of the elastomer. Besides experiment 1, where we investigated the differences in cell adherence properties of the M726, M727 and M927, all other experiments with batches of PCUU different from the M927 merely functioned as an extra control group.

As the initial cell adherence experiments with equine chondrocytes showed poor adherence of the cells, we switched to ATDC5 cells since they are known for their excellent binding properties and still exhibit chondrogenic behaviour. However, when we later performed another experiment with equine chondrocytes (experiment 3) we actually obtained very decent adherence results. We must therefore conclude that culturing methods or cell source were the cause of the initial poor adhesion and not the inability of PCUU to bind equine chondrocytes. This flaw actually improved our quality of research as we did not test one cell type but three. The favorable results in all three cell type experiments strengthens the confidence in a favorable in vivo outcome as it is unknown which cells exactly cause cartilage regeneration [7]. Furthermore, the largest percentage of cells that adhered to the PCUU versus the well plate was found with cartilage progenitor cells (42.9 %), a cell type believed to initiate cartilage regeneration [23]. This abundant cell adherence is visually confirmed by Figure 14 showing the total area of the PCUU construct covered with DAPI stained ACPC's. All together, this provides excellent cell binding prospects for the in vivo study.

Statistical tests were performed to evaluate the significant difference of our results. However, it can be questioned how reliable statistical tests such as an unpaired t-test or an one way ANOVA test are when using small sample sizes. Actually, in general, statistics in many publications can be questioned. John P.A. Ioannidis even goes as far as stating "*Most published research findings are false*" [56]. The statistical outcome is dependent on many factors such as; test of choice, sample size, group comparison of choice, and bias. It is therefore very difficult to draw the line of statistical significance and non statistical significance. Typically, this line relies on a significance level (α) of α= 0.05, where p-values below 0.05 indicate statistical significant difference and above non different. However, this threshold is arbitrary as the significance level can be set higher or lower depending on which research you study [57]. In this

research α= 0.05 was used as it is most common. However, the reliability of our conclusions based on p-values close to this threshold can be questioned. Low statistical power studies like ours reduce the chances of detecting a true effect. It can both lead to conclusions of statistical significant difference where none exists in reality as well as the other way around [58]. For instance, comparing M726 versus M927 in experiment 1 showed a p-value of 0.057, which is not a statistical significant difference. However, how clear is it that there is no statistical difference? Perhaps the same experiment with a larger sample size would point out significant difference. We should therefore be careful drawing conclusions from p-values approaching 0.05 with our small sample size.

Taken the above into account we cannot draw hard statistical significant conclusions from the results of experiment 1. However, we can observe that the mean average value of cells attached to the M927 PCUU versus the M726 and M727 is higher. Theoretically, this corresponds with literature findings. Firstly, M927 uses DMSO as a solvent during production compared to DMAc used in M726. DMAc induces a far greater toxic response to cells compared to DMSO in low concentrations [59] [60]. As it cannot be assured that absolutely no solvent residues are present in the PCUU, DMSO should be more "cell friendly" than the DMAc. Secondly, M927 is produced without a tin catalyst, which is used in both M726 and M727. Tin is known to have toxic effect on cells and tin residues are therefore undesired to be present in the elastomer [61]. Taken these literature findings into account together with the higher mean average value of M927 versus M726 and M727 makes the production optimization of replacing DMAc by DMSO and removing the tin catalyst is justified. Although not officially significantly different, all signs point towards superior cell binding properties of the M927 versus the M726 and M727.

Cell adherence properties of the PCUU were evaluated by comparing how many cells adhered to the well plate versus the PCUU construct. It was chosen that the potential surface area to adhere on was identical to the total surface area of the well plate and the PCUU construct individually. However, this is not a true reflection of reality. When cells are seeded in the well plate from suspension they encounter gravity and descend to the bottom ending up either on top of the PCUU construct or on the bottom of the well plate, rather than the sides of the construct. From there cells start to adhere and proliferate and can attach to the side of the PCUU as well. Nonetheless, this makes the side less prone to cell attachment. Besides that, the PCUU construct is not fixed to the well plate and can move around freely through the well making it possible for cells to adhere on the bottom of the PCUU as well as the well plate area below the construct. During the removal of the construct out of the well it is unknown what portion of cells adheres to the PCUU and what portion to the well plate area underneath the construct. Taken both circumstances into account, it was decided that the closest approximation could be achieved by designating all surface areas as potential surface area to adhere on. Bearing in mind that the growth area of the cell culture well plates are optimized for cell attachment and still a large portion of cells adhered to the PCUU, experiment 1, 2, and 3 show excellent results [62].

To really anchor the neo-tissue layer on top of the implant, more than just cell adherence is necessary. Porous PCUU architectures allowing ingrowth of tissue was investigated by 3D printing and punching holes. Proper printability of the PCUU solvent was found to be challenging and demanded a great deal of optimization. Furthermore, the formation of gas bubbles after printing due to evaporation of the solvents was worrisome since the solvents are toxic to cells. After a thorough optimization process both the printability and bubble formation could be controlled adequately and proper medium-resolution prints with 32 layers were achieved. However, to produce more complex and higher resolution 3D prints more research has to be done. Therefore, the main focus on in vitro tissue anchoring experiments layed on punched holes. To determine the optimal diameter of them, the outcome of experiment 5 relied on the percentile coverage of cells in a designated area. This was done as the indivual cells could not be quantified due to clustering. Since the average ACPC size should be similar in all three diameters, our approach of percentile coverage should deliver trustworthy results. Both 319 μm and 741 μm had a significantly larger percentile coverage of cells than the 188 μm. Although not statistically significant, the highest mean score was found in the 319 μm holes. This is in line with literature findings described in section 2.4 where 300-500 μm pores were found to be optimal for chondrocyte ingrowth and behaviour [33], [14], [34]. Considering this range, the 741 μm diameter performed very well being significantly out of the expected optimal range. We therefore hypothesize that the optimal diameter for cell ingrowth lies somewhere between 319 and 741 μm, further research should prove our hypothesis.

Besides the largest percentage of cells covering the shaft area, more aspects are important for choosing the opti-

mal diameter. Firstly, cells should be able to quickly fill the complete diameter and length of the hole to ensure proper anchoring. Secondly, more holes per surface area provides increased anchoring points leading to an improved distribution of anchor points providing superior resistance against stresses in multiple directions. Lastly, cartilage phenotype and extracellular matrix production have previously been reported to change in different hole diameters. A 270 μm hole diameter was found to be optimal to produce cartilage like tissue that produced collagen type II and GAGs. Larger diameter holes (620 μm) were found to generate inferior fibrous cartilage tissue producing less collagen type II and GAGs compared to the 270 μm [32]. All three arguments are in favor of the 319 μm holes compared to the 741 μm holes. One of the initial concerns of tinier holes was the capability of cartilage to diffuse nutrients all the way to the bottom of very narrow holes. However, according to Maroudas et al. nutrient diffusion should not be an issue in any of the holes as nutrients can diffuse from the synovial fluid into the cartilage up to 3.0 mm in depth [63]. The total depth of the implant consisting of a 0.8 mm deep hole together with a 0.5 mm layer of neo-tissue on top (total 1.3 mm) is not expected to be troublesome. As it was decided to use only one diameter hole for the in vivo study, one had to be chosen. Taken the highest mean average score of the 319 μm hole into account together with the arguments above, 319 μm was chosen for future in vivo studies.

It is fundamental for a permanent implant to not evoke a toxic or immunological response when exposed to the body or bodily fluids. In vitro experiments can test this to a certain extend. Experiment 6, where the cytotoxicity of 3D printed constructs was analysed with a MTT assay is one of these methods. No cytotoxic effect on cells was found caused by 3D printed constructs. This was however performed in a static test. One of the major concerns of the 3D prints is the presence of trapped evaporated solvent bubbles. During loading these bubbles may burst releasing potential toxic gasses into the body. Future experiments where mechanical loading of the 3D prints is combined with cell culturing is necessary to validate the biocompatibility of the 3D printed constructs further. Another tests performed to determine the biocompatibility of the PCUU constructs and 3D prints is the whole blood assay. Excellent results were derived as none of the plain, holes or 3DP PCUU's stood out of the negative control in any of the cytokines. Although in vitro results are promising, in vivo studies should determine the actual biocompatibility of the elastomer.

One of the key features of the elastomer part of the implant is the proposed similarity in mechanical properties with native cartilage. In order to compare mechanical properties of different elastomers and native cartilage, a comparable type of elastic modulus should be found. As a results of the viscoelastic properties of both the elastomer and native cartilage, an equilibrium modulus was sought after. For the elastomers, the stress relaxation moduli in G(1800) were determined as the compressive equilibrium modulus since after 30 minutes stress was approaching equilibrium. However, our tests with fresh equine cartilage were fruitless as the samples dried out quickly during testing. Literature was therefore consulted to find a comparable human cartilage modulus. The closest comparable modulus was found in a paper by Mow et al. who performed stress relaxation tests on human cartilage determining the intrinsic aggregate stress relaxation modulus [51]. This modulus is determined at the point of a stress relaxation test where fluid has ceased flowing through the cartilage and equilibrium is reached. It is therefore comparable to our compressive equilibrium modulus. Mow et al. found this modulus to be 0.76 MPa. As the goal of the elastomer part is to approach native cartilage, the goal for the compressive equilibrium modulus was set to be 1.0 MPa.

Korthagen et al. mentioned that their elastomer had mechanical properties approaching that of native cartilage [19]. However, our DMA tests have found very different properties for both their elastomer and our new PCUU. Previous similar mechanical tests by Korthagen et al. found that the Symo-Chem elastomer exhibited a compressive equilibrium modulus (G1800) of 3.14 MPa, where we found this to be 13.19 MPa. This could be due to the three-year improper storage of the material where UV and dehydration might have affected the elastomer. Therefore, our results on the Symo-Chem elastomer might not be a true reflection of its former mechanical properties. Even so, a G(1800) of 3.14 MPa is still more than four times that of native articular cartilage and it can be discussed if it matched the term "*approaching the mechanical properties of native cartilage*". More importantly are the mechanical properties of the M927. Its G(1800) was found to be 10.34 MPa which is far larger than that of native cartilage (0.76 MPa). Reducing this modulus by creating vertical aligned punched holes was found to be unfeasible. However, we did not discuss combining these vertical aligned holes with interconnecting horizontal holes from the sides. This would drastically reduce the equilibrium modulus as side holes would remove large parts of the vertical PCUU pillars providing mechanical strength. It would also improve the anchoring potential of the implant. However, creating

side holes extended the scope of our research as they should perfectly interconnect with the vertical holes to ensure evenly distributed mechanical properties and proper diffusion of nutrients. This was unfeasible as the holes were hand punched and creating more than 14 vertically aligned 500 μm holes in a 6 mm diameter sample was already very challenging, let alone create many more holes with perfectly interconnecting horizontal side holes. Future research with more advanced hole creation methods should determine the feasibility of this concept.

3D printing with interfacial layers was found to be feasible to approach the mechanical properties of native cartilage while being in the range of optimal pore sizes for cell ingrowth and adherence. This was based on the stress relaxation tests performed on a 32-layered M927 3D print. To reach the goal of a 1.0 MPa modulus the resolution of the print has to increase significantly. The combination of both reducing the wall thickness and the pore size is thought to be challenging due to the tough printability of the solved PCUU. However, certainly not impossible as according to our calculations we can already feasibly reach a pore size of 250 μm. This leaves room for lower resolution infill pattern and/or larger wall thickness making printing even more feasible. Besides that, the current infill used is rectangular. Other infills such as honeycomb or triangular should be investigated to achieve proper mechanical properties while providing excellent cartilage cell circumstances. Future 3D printing experiments should determine the feasibility of 3D printing as a solution to create the porous elastomer part of the implant.

In both punching holes and 3D printing the elastic modulus was determined regarding an "empty" structure. In vivo, the porous structure should be filled and covered with cartilage (like) tissue over time which will alter the mechanical properties along the way. Since the implant is directly part of the cartilage tissue and its mechanics after implantation, the implant should deliver proper mechanical strength straight away. As a results, the final compressive equilibrium modulus will be higher than the "empty" elastomer part of the implant before implantation. This is preferred to a too flexible implant directly after implantation as it can be deformed during loading by the surrounding cartilage leading to poorer ingrowth and binding properties.

The first equine in vivo trials will be performed with an implant with an elastomer part containing 14, 319 μm aligned vertical holes. These holes are created with a 500 μm micro punch. Figure 11 shows the cross section of how these will look. At initial contact the hole diameter will be 500 μm which quickly converges to 319 μm when entering the PCUU further. This causes a convex shape at the top part of the elastomer's hole. This can be used to our advantage by flipping the elastomer part upside down for the production of the in vivo implant. This convex shape at the bottom of the hole will result in improved anchoring after ingrowth of tissue. This will subsequently results in extra resistance against detachment by shear forces increasing the quality of our implant. The in vivo results will be extremely valuable to verify our in vitro outcomes. When successful, this could be a huge step forwards in the functional treatment of osteochondral defects and degenerative joint diseases. It can therefore have an enormous societal impact as so many people suffer from these defects and diseases worldwide.

5 Conclusion

The in vitro outcomes of this study are promising for future in vivo experiments. The poor in vivo binding properties of the previously used elastomer in the study by Korthagen et al. were tackled by a newly produced PCUU elastomer and creating porosity. Both 3D printing and punching holes have great potential in creating porosity and physically anchoring the neo-tissue that grows into the elastomer part of the implant. Besides excellent cell facilitating properties, the PCUU is desired to approach the mechanical properties of native articular cartilage. However, the compressive equilibrium modulus of PCUU was found to be significantly higher than native cartilage. Nonetheless, By creating porosity this modulus could be reduced to match native cartilage.

The optimal diameter of vertically aligned punched holes was found to be 319 μm. Not only provided this diameter optimal circumstances for cartilage to grow into, it also optimized anchoring potential. However, it was proved to be unfeasible to achieve the desired mechanical properties by just creating vertically aligned holes. Future research with interconnecting horizontal side holes should be conducted to reduce stiffness of the PCUU construct even further to approach that of native cartilage. 3D printing techniques were found to be feasible in providing both excellent cell facilitating properties as mechanical properties. Although decent 3D printed constructs were produced and tested

in this study, further research is needed to produce higher resolution prints to function as the elastomer part of the implant in vivo.

Both punched and 3D printed PCUU samples were tested for toxicity and immune response. Both tests derived excellent results and no signs of toxicity or undesired immune response was detected. These results combined with the excellent cell binding properties of the PCUU strengthens our confidence in favorable in vivo outcomes. Future in vivo trials should verify our hopeful in vitro results.

References

[1] Michiel W. Pot, Veronica K. Gonzales, Pieter Buma, Joanna IntHout, Toin H. van Kuppevelt, Rob B.M. de Vries, and Willeke F. Daamen. Improved cartilage regeneration by implantation of acellular biomaterials after bone marrow stimulation: a systematic review and meta-analysis of animal studies. *PeerJ*, 4:e2243, sep 2016.

[2] Ji-Hyun Ahn, Tae-Hyeong Lee, Jong-Soo Oh, Su-Yeon Kim, Hyun-Jung Kim, Il-Kyu Park, Baek-Sun Choi, and Gun-Ii Im. A novel hyaluronate–atelocollagen/β-tcp–hydroxyapatite biphasic scaffold for the repair of osteochondral defects in rabbits. *Tissue Engineering Part A*, 15(9):2595–2604, 2009.

[3] Weili Shi, Muyang Sun, Xiaoqing Hu, Bo Ren, Jin Cheng, Chenxi Li, Xiaoning Duan, Xin Fu, Jiying Zhang, Haifeng Chen, et al. Structurally and functionally optimized silk-fibroin–gelatin scaffold using 3d printing to repair cartilage injury in vitro and in vivo. *Advanced Materials*, 29(29):1701089, 2017.

[4] PJ Reardon, R Konwarh, JC Knowles, BB Mandal, et al. Mimicking hierarchical complexity of the osteochondral interface using electrospun silk-bioactive glass composites. *ACS applied materials & interfaces*, 9(9):8000–8013, 2017.

[5] AJ Nixon, LA Fortier, LR Goodrich, and NG Ducharme. Arthroscopic reattachment of osteochondritis dissecans lesions using resorbable polydioxanone pins. *Equine veterinary journal*, 36(5):376–383, 2004.

[6] Yingying Du, Haoming Liu, Qin Yang, Shuai Wang, Jianglin Wang, Jun Ma, Insup Noh, Antonios G Mikos, and Shengmin Zhang. Selective laser sintering scaffold with hierarchical architecture and gradient composition for osteochondral repair in rabbits. *Biomaterials*, 137:37–48, aug 2017.

[7] Daniel J Huey, Jerry C Hu, and Kyriacos A Athanasiou. Unlike bone, cartilage regeneration remains elusive. *Science*, 338(6109):917–921, 2012.

[8] Silvia Panseri, Alessandro Russo, Carla Cunha, Alice Bondi, Alessandro Di Martino, Silvia Patella, and Elizaveta Kon. Osteochondral tissue engineering approaches for articular cartilage and subchondral bone regeneration. *Knee Surgery, Sports Traumatology, Arthroscopy*, 20(6):1182–1191, 2012.

[9] F Raquel Maia, Mariana R Carvalho, J Miguel Oliveira, and Rui L Reis. Tissue Engineering Strategies for Osteochondral Repair. *Advances in experimental medicine and biology*, 1059:353–371, 2018.

[10] Gian M Salzmann, Martin Sauerschnig, Markus T Berninger, Theresa Kaltenhauser, Martin Schönfelder, Stephan Vogt, Gabriele Wexel, Thomas Tischer, Norbert Sudkamp, Philipp Niemeyer, et al. The dependence of autologous chondrocyte transplantation on varying cellular passage, yield and culture duration. *Biomaterials*, 32(25):5810–5818, 2011.

[11] Maurilio Marcacci, Elizaveta Kon, Marco Delcogliano, Giuseppe Filardo, Maurizio Busacca, and Stefano Zaffagnini. Arthroscopic autologous osteochondral grafting for cartilage defects of the knee: prospective study results at a minimum 7-year follow-up. *The American journal of sports medicine*, 35(12):2014–2021, 2007.

[12] Syam P Nukavarapu and Deborah L Dorcemus. Osteochondral tissue engineering: current strategies and challenges. *Biotechnology advances*, 31(5):706–21, sep 2013.

[13] László Hangody, Jozsef Dobos, Eszter Baló, Gergely Pánics, Laszlo Rudolf Hangody, and Istvan Berkes. Clinical experiences with autologous osteochondral mosaicplasty in an athletic population: a 17-year prospective multicenter study. *The American journal of sports medicine*, 38(6):1125–1133, 2010.

[14] Shuaijun Jia, Jing Wang, Ting Zhang, Weimin Pan, Zhong Li, Xin He, Chongfei Yang, Qining Wu, Wei Sun, Zhuo Xiong, and Dingjun Hao. Multilayered Scaffold with a Compact Interfacial Layer Enhances Osteochondral Defect Repair. *ACS applied materials & interfaces*, 10(24):20296–20305, jun 2018.

[15] Elizaveta Kon, Giuseppe Filardo, Francesco Perdisa, Giulia Venieri, and Maurilio Marcacci. Clinical results of multilayered biomaterials for osteochondral regeneration. *Journal of experimental orthopaedics*, 1(1):10, dec 2014.

[16] Kirsty A Husby, Shannon K Reed, David A Wilson, Keiichi Kuroki, John R Middleton, Natalie C Hoepp, Elizabeth M Charles, and James L Cook. Evaluation of a permanent synthetic osteochondral implant in the equine medial femoral condyle. *Veterinary Surgery*, 45(3):364–373, 2016.

[17] Xuezhou Li, Jianxun Ding, Jincheng Wang, Xiuli Zhuang, and Xuesi Chen. Biomimetic biphasic scaffolds for osteochondral defect repair. *Regenerative Biomaterials*, 2(3):221–228, sep 2015.

[18] Diana Ribeiro Pereira, Rui L Reis, and J Miguel Oliveira. Layered Scaffolds for Osteochondral Tissue Engineering. *Advances in experimental medicine and biology*, 1058:193–218, 2018.

[19] NM Korthagen, H Brommer, G Hermsen, SGM Plomp, G Melsom, K Coeleveld, SC Mastbergen, H Weinans, W van Buul, and PR van Weeren. A short-term evaluation of a thermoplastic polyurethane implant for osteochondral defect repair in an equine model. *The Veterinary Journal*, page 105340, 2019.

[20] Kenton R Kaufman, Kai-Nan An, William J Litchy, Bernard F Morrey, and Edmund YS Chao. Dynamic joint forces during knee isokinetic exercise. *The American journal of sports medicine*, 19(3):305–316, 1991.

[21] Chisa Shukunami, Kiyoto Ishizeki, Tadao Atsumi, Yoshiyuki Ohta, Fujio Suzuki, and Yuji Hiraki. Cellular hypertrophy and calcification of embryonal carcinoma-derived chondrogenic cell line atdc5 in vitro. *Journal of Bone and Mineral Research*, 12(8):1174–1188, 1997.

[22] Sigmaaldrich. Atdc5, 2019.

[23] Gary P Dowthwaite, Joanna C Bishop, Samantha N Redman, Ilyas M Khan, Paul Rooney, Darrell JR Evans, Laura Haughton, Zubeyde Bayram, Sam Boyer, Brian Thomson, et al. The surface of articular cartilage contains a progenitor cell population. *Journal of cell science*, 117(6):889–897, 2004.

[24] Johan Van Meerloo, Gertjan JL Kaspers, and Jacqueline Cloos. Cell sensitivity assays: the mtt assay. In *Cancer cell culture*, pages 237–245. Springer, 2011.

[25] M O'neill, J McPartlin, K Arthure, S Riedel, and ND McMillan. Comparison of the tlda with the nanodrop and the reference qubit system. In *Journal of Physics: Conference Series*, volume 307, page 012047. IOP Publishing, 2011.

[26] Ewa Papierowska, Sylwia Szporak-Wasilewska, Joanna Szewińska, Jan Szatyłowicz, Guillaume Debaene, and Marta Utratna. Contact angle measurements and water drop behavior on leaf surface for several deciduous shrub and tree species from a temperate zone. *Trees*, 32(5):1253–1266, 2018.

[27] WS Ramsey, W Hertl, ED Nowlan, and NJ Binkowski. Surface treatments and cell attachment. *In vitro*, 20(10):802–808, 1984.

[28] Sarina Kay, Anil Thapa, Karen M Haberstroh, and Thomas J Webster. Nanostructured polymer/nanophase ceramic composites enhance osteoblast and chondrocyte adhesion. *Tissue engineering*, 8(5):753–761, 2002.

[29] Natasja Leth Joergensen, Dang Quang Svend Le, Ole Zoffmann Andersen, Morten Foss, Carl Christian Danielsen, Casper Bindzus Foldager, Martin Lind, and Helle Lysdahl. Topography-guided proliferation: distinct surface microtopography increases proliferation of chondrocytes in vitro. *Tissue Engineering Part A*, 21(21-22):2757–2765, 2015.

[30] SV Prasad, C Pavithran, and PK Rohatgi. Alkali treatment of coir fibres for coir-polyester composites. *Journal of materials science*, 18(5):1443–1454, 1983.

[31] M Lampin, R Warocquier-Clérout, C Legris, M Degrange, and MF Sigot-Luizard. Correlation between substratum roughness and wettability, cell adhesion, and cell migration. *Journal of Biomedical Materials Research: An Official Journal of The Society for Biomaterials and The Japanese Society for Biomaterials*, 36(1):99–108, 1997.

[32] Yun-Jeong Seong, In-Gu Kang, Eun-Ho Song, Hyoun-Ee Kim, and Seol-Ha Jeong. Calcium Phosphate-Collagen Scaffold with Aligned Pore Channels for Enhanced Osteochondral Regeneration. *Advanced Healthcare Materials*, 6(24):1700966, dec 2017.

[33] Sio-Mei Lien, Liang-Yu Ko, and Ta-Jen Huang. Effect of pore size on ecm secretion and cell growth in gelatin scaffold for articular cartilage tissue engineering. *Acta biomaterialia*, 5(2):670–679, 2009.

[34] Tanya J Levingstone, Emmet Thompson, Amos Matsiko, Alexander Schepens, John P Gleeson, and Fergal J O'Brien. Multi-layered collagen-based scaffolds for osteochondral defect repair in rabbits. *Acta biomaterialia*, 32:149–160, mar 2016.

[35] Scott J Hollister. Porous scaffold design for tissue engineering. *Nature materials*, 4(7):518, 2005.

[36] Dietmar W Hutmacher. Scaffolds in tissue engineering bone and cartilage. In *The biomaterials: Silver jubilee compendium*, pages 175–189. Elsevier, 2000.

[37] Martha O Wang, Charlotte E Vorwald, Maureen L Dreher, Eric J Mott, Ming-Huei Cheng, Ali Cinar, Hamidreza Mehdizadeh, Sami Somo, David Dean, Eric M Brey, et al. Evaluating 3d-printed biomaterials as scaffolds for vascularized bone tissue engineering. *Advanced Materials*, 27(1):138–144, 2015.

[38] Jeffrey W Stansbury and Mike J Idacavage. 3d printing with polymers: Challenges among expanding options and opportunities. *Dental Materials*, 32(1):54–64, 2016.

[39] Lawrence Livermore National Library. 3d-printed aerogels improve energy storage, 2015.

[40] Tony McNally. *Polymer modified bitumen: Properties and characterisation*. Elsevier, 2011.

[41] AZO materials. How do dynamic mechanical analyzers work?, 2015.

[42] Dinorath Olvera, Andrew Daly, and Daniel John Kelly. Mechanical testing of cartilage constructs. In *Cartilage Tissue Engineering*, pages 279–287. Springer, 2015.

[43] Douglas G Altman and J Martin Bland. Statistics notes: the normal distribution. *Bmj*, 310(6975):298, 1995.

[44] Jogikalmat Krithikadatta. Normal distribution. *Journal of conservative dentistry: JCD*, 17(1):96, 2014.

[45] JF McCabe and TE Carrick. A statistical approach to the mechanical testing of dental materials. *Dental Materials*, 2(4):139–142, 1986.

[46] Craig Snoeyink, Sourav Barman, and Gordon F Christopher. Contact angle distribution of particles at fluid interfaces. *Langmuir*, 31(3):891–897, 2015.

[47] Clinical Research Clinic AMC. Keuze toets, 2017.

[48] Greiner Bio-One. Cellstar® zellkultur multiwell platten, 2019.

[49] Math central. I have the actual length of an arc plus the length of the cord. how do i determine the radius of the arc., 2019.

[50] Dolores Silva, Carlos GG Ponte, Mariana A Hacker, and Paulo RZ Antas. A whole blood assay as a simple, broad assessment of cytokines and chemokines to evaluate human immune responses to mycobacterium tuberculosis antigens. *Acta tropica*, 127(2):75–81, 2013.

[51] Van C Mow, SC Kuei, W Michael Lai, and Cecil G Armstrong. Biphasic creep and stress relaxation of articular cartilage in compression: theory and experiments. *Journal of biomechanical engineering*, 102(1):73–84, 1980.

[52] Engineering Toolbox. maller circles within a larger circle, 2019.

[53] Lorna J Gibson and Michael F Ashby. *Cellular solids: structure and properties*. Cambridge university press, 1999.

[54] F López Jiménez and N Triantafyllidis. Buckling of rectangular and hexagonal honeycomb under combined axial compression and transverse shear. *International Journal of Solids and Structures*, 50(24):3934–3946, 2013.

[55] Mingyan Zhao, Lihua Li, Xian Li, Changren Zhou, and Bo Li. Three-dimensional honeycomb-patterned chitosan/poly (l-lactic acid) scaffolds with improved mechanical and cell compatibility. *Journal of biomedical materials research part A*, 98(3):434–441, 2011.

[56] John PA Ioannidis. Why most published research findings are false. *PLoS medicine*, 2(8):e124, 2005.

[57] Yale University. Tests of significance, 1997.

[58] Katherine S Button, John PA Ioannidis, Claire Mokrysz, Brian A Nosek, Jonathan Flint, Emma SJ Robinson, and Marcus R Munafò. Power failure: why small sample size undermines the reliability of neuroscience. *Nature Reviews Neuroscience*, 14(5):365, 2013.

[59] Tae Sung Choi, Kuck Hyeun Woo, Jin Seok Kim, Wan Seup Park, Jung Ho Ham, Sang Je Jung, and Jae Young Yu. Toxic hepatitis induced by occupational dimethylacetamide exposure. *Korean Journal of Occupational and Environmental Medicine*, 13(2):164–170, 2001.

[60] Georges Da Violante, Naima Zerrouk, Isabelle Richard, Gérard Provot, Jean Claude Chaumeil, and Philippe Arnaud. Evaluation of the cytotoxicity effect of dimethyl sulfoxide (dmso) on caco2/tc7 colon tumor cell cultures. *Biological and pharmaceutical bulletin*, 25(12):1600–1603, 2002.

[61] KA Winship. Toxicity of tin and its compounds. *Adverse drug reactions and acute poisoning reviews*, 7(1):19–38, 1988.

[62] Greinerbioone. Cellstar® cell culture dishes, 2019.

[63] Alice Maroudas, PETER Bullough, SAV Swanson, and MAR Freeman. The permeability of articular cartilage. *The Journal of bone and joint surgery. British volume*, 50(1):166–177, 1968.

[64] Rebecca Williams, Ilyas M Khan, Kirsty Richardson, Larissa Nelson, Helen E McCarthy, Talal Analbelsi, Sim K Singhrao, Gary P Dowthwaite, Rhiannon E Jones, Duncan M Baird, et al. Identification and clonal characterisation of a progenitor cell sub-population in normal human articular cartilage. *PloS one*, 5(10):e13246, 2010.

[65] Thermofisher. Qubit dsdna br assay kit, 2019.

6 Appendix

6.1 Equine chondrocytes

The equine chondrocytes used were previously isolated under sterile conditions from macroscopically healthy stifle joints of warmblood horses that were euthanisedin the Department of Equine Sciences, Faculty of Veterinary Medicine, Utrecht University, the Netherlands. Cartilage was digested overnight in type II collagenase (Worthington Biochemical Corporation) at 37°C and the resulting cell suspension was filtered and washing in phosphate-buffered saline (PBS, Gibco, USA) and stored in liquid nitrogen until use. Two different donors were used in our experiments.

1. EQ031, P0, sp 12-08-2015
2. EQ033, P0, sp 13-08-2015

Both donors were cultured with cell culture medium consisting of: Dulbeccos Modified Eagle Medium (DMEM)(high glucose, GlutaMAX^{TM}, pyruvate) (Gibco, USA) with 10% Fetal Bovine Serum (FBS) (Biowest, France), 10 μl/ml penicillin/streptomycin (pen/strep)(Gibco, USA), 5μl/ml l-ascorbic acid-2-phosphate (ASAP)(Sigma, USA), 1μl/ml beta-Fibroblast Growth Factor (β-FGF)(R&D Systems, USA), and 5μl/ml Fungizone (Gibco, USA). From now on referred to as "chondrocyte medium".

6.2 ATDC5 cells

ATDC5 cells were in stock in the Hubrecht laboratory and years ago received from another department. No official source is known. ATDC5 cells were cultured with: DMEM (high glucose, GlutaMAX^{TM}, pyruvate) (Gibco, USA) with 10% FBS (Biowest, France) and 1 μl/ml pen/strep (Gibco, USA). From now on referred to as "ATDC5 medium".

6.3 Equine articular cartilage progenitor cells

Our equine cartilage progenitors were isolated from healthy donor cartilage that was harvested in the same way as described in Appendix "Equine chondrocytes". The sample used was EQ 19.002 P0. Before storing the donor equine chondrocytes in liquid nitrogen an aliquot of the total harvest was used to isolate the progenitors. The aliquot was plated down as a full-depth chondrocyte population (total cell mass from surface, mid and deep zones) and subjected to a fibronectin adhesion assay as described by Williams et al. [64]. Afterwards, six well plates were coated with 10 mg/ml fibronectin (FN) (Sigma, UK) in 0.1 M phosphate buffered saline (PBS, pH7.4) (Gibco, USA) containing 1 mM $MgCl_2$ and 1 mM $CaCl_2$ overnight at 4°C. Isolated full-depth chondrocytes (4000 cells/ml) were seeded onto the coated plates for 20 min at 37°C in DMEM. After 20 mins, media and nonadherent cells were removed. All adherent cells were afterwards harvested and considered as ACPCs.

Equine cartilage progenitors were cultured with: DMEM (high glucose, GlutaMAX^{TM}, pyruvate) (Gibco, USA) with 10% FBS (Biowest, France), 10μl/ml pen/strep (Gibco, USA), 5μl/ml ASAP (Sigma, USA), and 1μl/ml β-FGF (R&D Systems, USA). From now on referred to as "progenitor medium".

6.4 Surface treatments

Goal

Test multiple M524 PCUU surface treatments to improve ATDC5 cell binding properties and/or hydrophilicity.

Materials and methods

- PCUU (M524)
- Symo-Chem elastomer
- ATDC5 P18, 11/11/18
- Constructs sterilized with UV in the UV crosslinker at 39.5 mJ/cm^2 both sides

- Mili-Q water
- ATDC5 medium
- 10 ml glass vial with lid
- Surface treatments:
  - 0.1% TFA in DCM (5 min), (Sigma-Aldrich, USA) (Honeywell, USA)
  - 100% DCM (5 min), (Honeywell, USA)
  - Alkali (NaOH, 5M, 60 °C, 8 hours), (Sigma-Aldrich, USA)
  - 100% Chloroform (5 min), (VWR chemicals, the Netherlands)

PCUU samples were first treated with the surface treatment in the stated concentrations and time. Afterwards all PCUU samples were washed in a mili-Q water bath overnight at 40 °C. Afterwards they were sterilized with UV. As a control, an untreated M524 sample was taken into research. Ethanol, and EtO sterilized samples were included as well to investigate whether sterilization method had obvious influence. All test were done with n=1. Results were analyzed with the DNA Qubit, please see Appendix "DNA Qubit assay" for details. Wettability tests were performed as well to investigate whether this had influence on cell binding properties.

Results

Results for the Qubit assay can be seen in Figure 23. Results for the wettability test can be found in Figure 24. As n=1 we were searching for outstanding results which we could build on in further research. However, no outstanding improvement in cell binding was found in any of the surface treatment. Besides that, no obvious correlation between cell binding properties and wettability was found. We therefore terminated this side track of research.

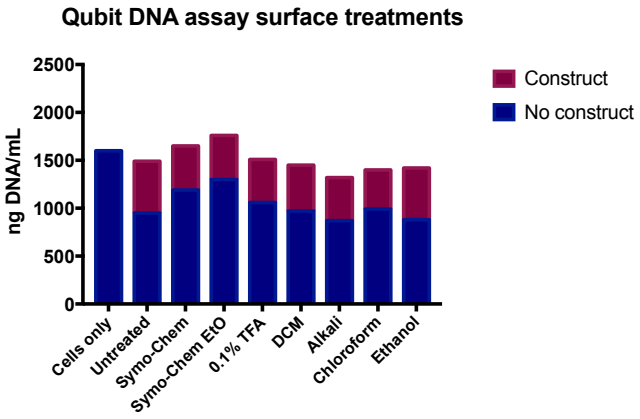

Figure 23: displaying the ng DNA/mL detected in the control well and the different PCUU sample wells for ATDC5 cells. PCUU bars show distinction between the proportion of cells adhered to the well plate (no construct) and the proportion adhered to the construct (construct).

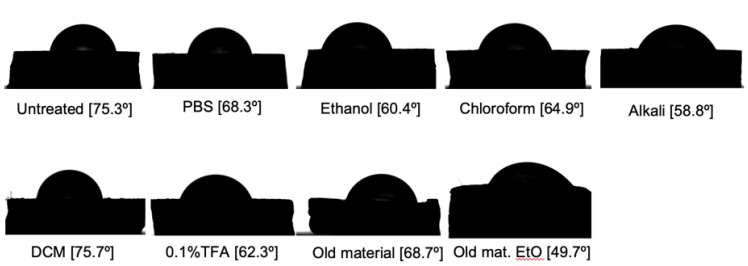

Figure 24: Wettability results of different surface treatments. Data derived from the OCA 15EC.

6.5 3D print optimizations

Goal

Optimize the printability of M727 PCUU with different TFA/DCM concentrations and PCUU/solvent ratios.

Materials and methods

- M727 PCUU
- TFA
- DCM
- 10ml glass vial with lid
- 3ml bioprint cartridge
- 27G transparent nozzle

Seven different ratios were used and analyzed:

1. 400mg PCUU in 2ml 50/50% TFA/DCM
2. 400mg PCUU in 2ml 10/90% TFA/DCM
3. 350mg PCUU in 2ml 10/90% TFA/DCM
4. 350mg PCUU in 2ml 5/95% TFA/DCM
5. 360mg PCUU in 2ml 10/90% TFA/DCM
6. 360mg PCUU in 2ml 5/95% TFA/DCM
7. 360mg PCUU in 2ml 2/95% TFA/DCM

This experiment consisted on two test. Firstly, can the solvent completely dissolve the PCUU homogeneously, Secondly, how many and how large bubbles are formed after printing. The same eight-layered print was performed with all different mixtures, Figure 25, 26. The parameters used were; pressure: 79 KPa, print speed: 15 mm/s, layer height: 0.03mm. Results were optically analyzed.

Results

From the first test it became apparent that any concentration of TFA below 5% were not capable of solving the PCUU completely and anything above 10% was too aggresive as it turned a more yellowish colour and it affected the print nozzle. Besides that, 350mg PCUU led to a too liquid gel and was removed as a potential optimal mixture. During bubble tests we found that all 10% TFA mixtures caused significantly more bubbles than the 5% TFA, Figure 25, 26. Least bubbles were found with a mixture of 360mg PCUU 5% TFA/DCM. Further optimization is necessary to find the absolute optimimum.

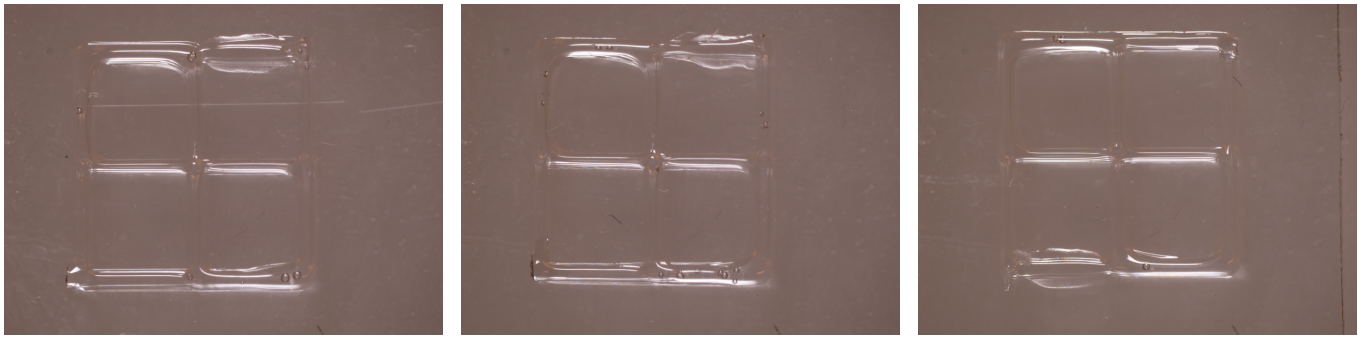

Figure 25: 8-layered 3D print with 360 mg PCUU in 5% TFA/DCM.

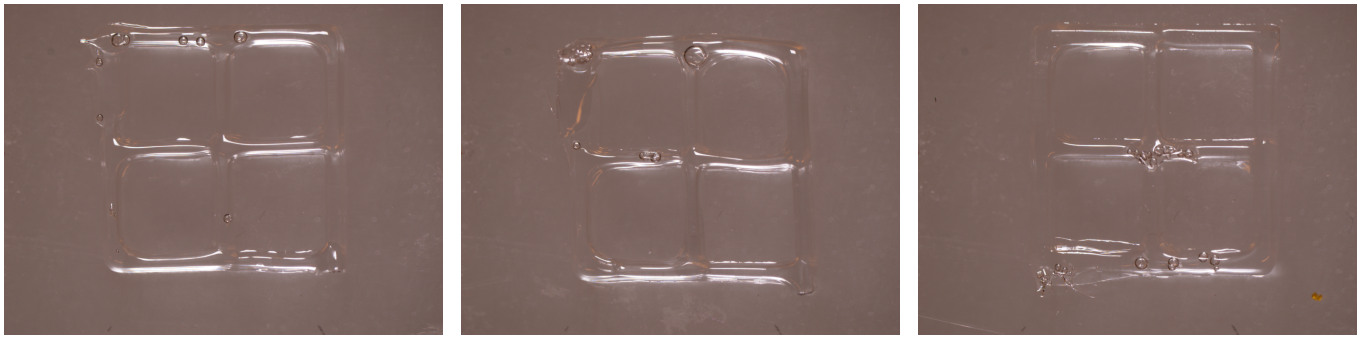

Figure 26: 8-layered 3D print with 360 mg PCUU in 10% TFA/DCM.

6.6 3D print wash protocol

Goal

Remove residue solvents from 3DP PCUU constructs

Materials and method

- Vacuum machine
- 70% ethanol
- Mili-Q water
- Constructs sterilized with UV in the UV crosslinker at 39.5 mJ/cm^2 both sides
- Plain DMEM medium with 1 % p/s
- 20 ml glass vial with lid
- magnetic stirring rod

Place the construct in the vacuum machine at 600mbar for 1h directly after printing. Wash the scaffold overnight with 15 ml, 70% ethanol with a stirring rod at 300rpm. Take out the construct and wash for 2h with 15 ml Mili-Q water and change to a fresh batch of water and leave overnight, again add a stirring rod at 300rpm. Sterilize the construct for 30 min per side with UV (39.5 mJ/cm ^{2}). Leave the samples in 2 ml medium for a minimum of 24h and change medium once a day and at least twice in total.

6.7 MTT assay

Materials and methods

- Thiazolyl blue tetrazolium bromide (Sigma-Aldrich, USA)
- Plain DMEM medium
- DMSO (Honeywell, USA)
- VersaMax reader (Molecular Devices, USA)

Make a 0.5 mg/ml solution of thiazolyl in DMEM and push through a 0.22 μm filter to make sterile. Aspirate the medium from the cell culture wells and add 100 μl (96-well) or 300 μl (48 well) of the solution to each well. Incubate for 2 hours at 37 °C in an incubator with 21 % O_2, 5% CO_2. After 2 hours, aspirate the solution and add 100/300 μl DMSO to each well. Incubate under same circumstances for 30 minutes. Add in the same amount of wells as the sample size plain DMEM as a negative control and measure outcome values in the VersaMax (Molecular Devices, USA). If a 48-well was used, transfer the volume of each well evenly over two 96-wells as the Versamax only reads out 96-wells plates. Settings Versamax: Endpoint, wavelength: 595 nm, shake 2 sec before reading.

6.8 DNA Qubit assay

Materials and methods

- HBSS (Gibco, USA)
- 0.05 % Trypsin EDTA 1x (Gibco, USA)
- DMEM with FBS
- TE buffer with 0.1% Triton (Sigma-Aldrich, USA)
- Qubit dsDNA BR assay kit (Invitrogen, USA)
- Qubit 2.0 Fluorometer (Invitrogen, USA)

After the appropriate culturing time, take out the PCUU constructs out of the well with sterile tweezers and place in a new clean well. Wash both the constructs and the original well twice with HBSS and remove. Add 300 μl (96-well) or 500 μl (48-well) Trypsin per well and incubate for 10 min. Add 300/500 μl medium with FBS to trop the trypsin reaction. Transfer to a 1 ml vial and centrifuge at 500g for 5 min (2300 RPM Eppendorf centrifuge). Remove supernatant and resuspend in 100 μl TE buffer. Incubate the cells for 15 minutes on ice and vortex once. Start Qubit dsDNA BR assay according to the delivered protocol [65]. We used 20 μl sample to 180 μl working solution.

6.9 Wettability test

Materials and methods

- Demi water
- PCUU construct
- OCA 15EC (DataPhysics Instruments, Germany)

Place the PCUU sample in focus on the OCA machine and carefully pippet 5 μl of demi water on top of the construct (in the middle). Perform a sessile droplet test on the machine and let the software calculate the contact angle.

6.10 DAPI protocol

Materials and methods

- 1 mg/ml 4',6-diamidino-2-fenylindool (DAPI)
- PBS

Make a DAPI/PBS solution by adding 20 μl DAPI to 1980 μl PBS. Add 300 μl DAPI/PBS solution to each 48-well and incubate for 20 minutes. Aspirate the solution and wash once with PBS and add a new batch of 300 μl PBS. Image with a fluorescence microscope.

6.11 Whole blood assay

Blood of three healthy equine donors was collected using heparin as an anti-coagulant (Greiner Bio-One, VACUETTE ^{TM}lithium heparin tubes, 9 ml, catalog number 95057-415). The blood was diluted 6 times (v/v) with culture medium (RPMI 1640 glutamax without additives) and 600 μl was added to the wells of a 48 wells plate (Greiner bio-one, Cellstar 48 Well Cell Culture Plate, Cat.-No. 677 180). Materials were added to the wells and to control wells only containing medium. In the negative control only medium was added to the blood. lipopolysaccharide (LPS) was added as a positive control. The plate was then incubated for 18 hours in at 37 °C and with 5% CO2 in an incubator. The next day the contents of the wells were transferred into 1,5 mL eppendorf tubes and centrifuged at 500G for 5 minutes. The supernatant was transferred to micronic storage boxes and frozen at -80 °C until analysis.

Supernatants were analysed using enzyme-linked immunosorbent assays (ELISAs) against IL-8, CCL2, and TNF-α. IL-8 and CCL2 were do-it-yourself ELISA-kits from Kingfisher Biotech (KFDIY0702E003 and KFDIY0694E003, respectively) using in-house developed protocols based on the instructions provided by the supplier. TNF-α was measuring the ELISA kit from Thermo Scientific (ESS0017), according to the manufacturer's instructions. In short, coating antibody was diluted in carbonate-bicarbonate buffer, pH 9.6 and 100 μl was added to each well of Greiner Microlon 96-wells ELISA plates. After overnight incubation at room temperature, plates were emptied and blocked by filling them with PBS 1% Bovine Serum Albumin (BSA) and incubating for 2 hours. Then, plates were emptied and 100 μl of sample or standard was added to the wells and incubated for 1 hour. The standard was prepared in culture medium using a 2-fold dilution series. Plates were washed four times with PBS 0,05% Tween 20 and then 100ul of detection antibody diluted in PBS 1% BSA was added to the plates and incubated for 1 hour. After washing, 100ul of Streptavidin-HRP working solution (12.5 ng/ml) in PBS 1 % BSA was added for 30 minutes. After a final washing, 100 μl of ready-to-use TMB substrate solution was added for 20-40 minutes until sufficient color had developed followed by 100 μl of 0.18M H2SO4 stop solution. Absorbance was measured on a VERSAmax microplate reader (Molecular Devices) at 450 nm (with 540 nm measurement for background correction). Results were analysed by using a 4-parameter plot of the standard curve to calculate the sample values.

6.12 DMA results

Five different samples were tested for stress relaxation test in the DMA Q800 (TA instruments, USA). Their dimensions can be found in Table 4. Final results can be found in Table 5. Individual stress relaxation curves of the different samples van be found in Figure 27 - 31. Results of the cartilage sample are included in this appendix, but failed and are left out of consideration in the actual study.

Table 4: Dimensions of the tested samples for DMA test

Test	Description	Dimensions
1	Symo-Chem	∅ 3 x 2.93 mm
2	M901	∅ 3 x 1.46 mm
3	M927	∅ 3 x 1.43 mm
4	3DP M927	□ 8 x 0.80 mm
5	Equine cartilage	∅ 3 x 1.68 ± 0.13 mm (average of three specimens)

Table 5: Stress relaxation tests results, onset stress relaxation modulus (G(0) and compressive equilibirum modulus G(1800) are shown.

Test	Stress relaxation modulus (MPa)	
	G(0)	G(1800)
Symo-Chem	14.83 ± 0.20	13.19 ± 0.07
M901	15.47 ± 0.07	13.17 ± 0.34
M927	11.84 ± 0.25	10.34 ± 0.35
3DP M927	0.33 ± 0.05	0.22 ± 0.03
Equine cartilage	0.79 ± 0.25	0.04 ± 0.01

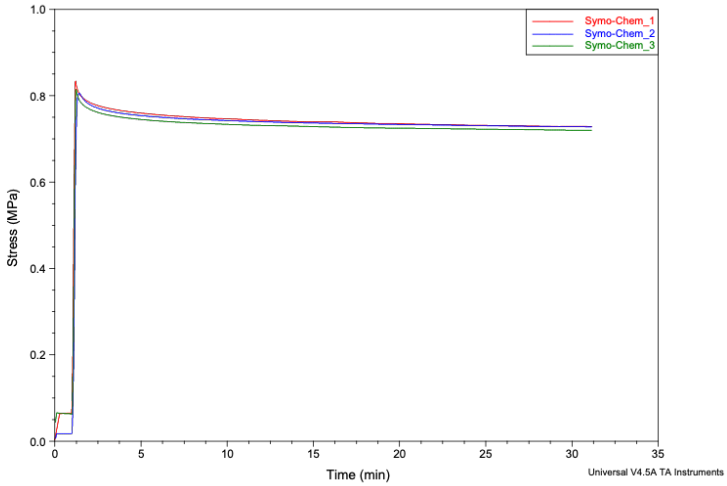

Figure 27: DMA Stress relaxation curves of Symo-Chem elastomer

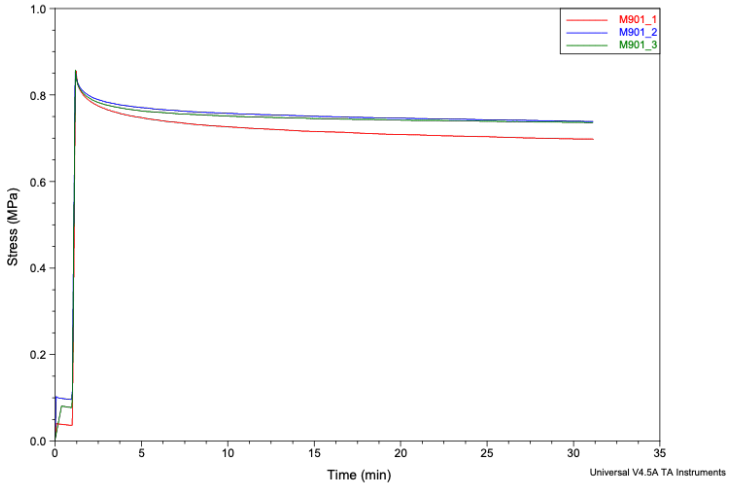

Figure 28: DMA Stress relaxation curves of M901 PCUU

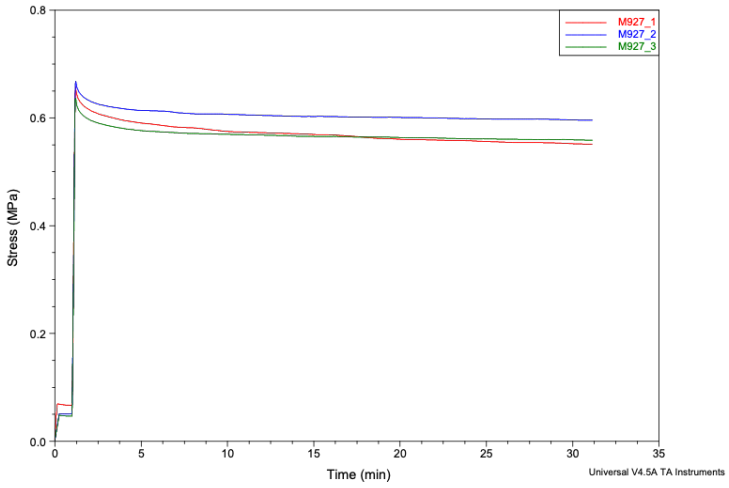

Figure 29: DMA Stress relaxation curves of M927 PCUU

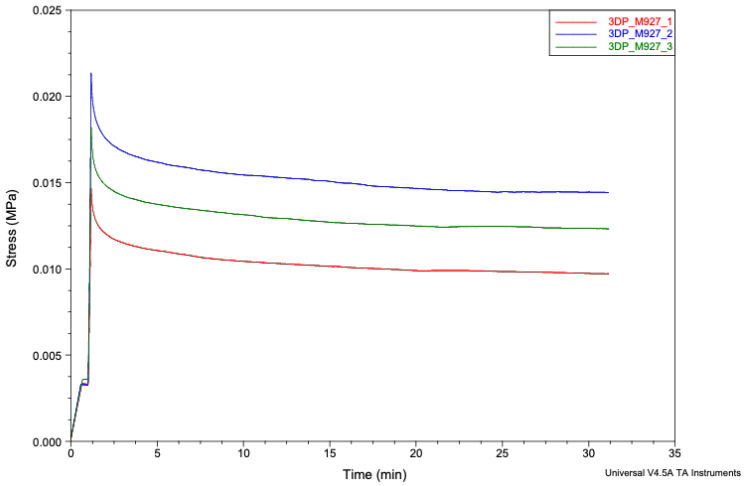

Figure 30: DMA Stress relaxation curves of M927 3DP

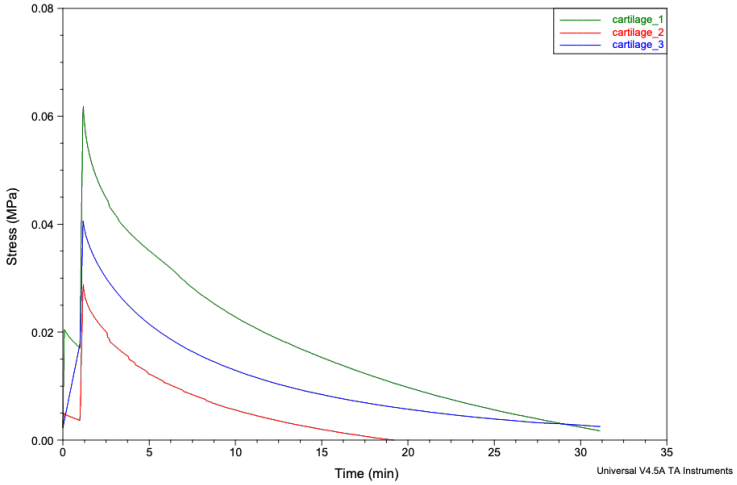

Figure 31: DMA Stress relaxation curves of equine cartilage